Czech Technical University in Prague
Faculty of Electrical Engineering
Department of Measurement

Measurement and Monitoring of Energy Consumption in Aviation: Diagnostics and Detection of Degradations

by

Ing. Ondřej Hanuš

Doctoral Thesis

Ph.D. programme: P2612 - Electrical Engineering and Information Technology
Branch of study: 3708V017 - Air Traffic Control
Supervisor: Prof. Ing. Radislav Šmíd, Ph.D.

February 2022

Supervisor:
Prof. Ing. Radislav Šmíd, Ph.D.
Department of Measurement
Faculty of Electrical Engineering
Czech Technical University in Prague
Technická 2
160 00 Prague 6
Czech Republic

Acknowledgements

First of all, I would like to thank my parents and the rest of the family for their love and great support during my studies. Special thanks go to my supervisor Prof. Radislav Šmíd, PhD. for his valuable advice and for leading the project that made this work possible. My thanks also go to other colleagues and members of the Faculty of Electrical Engineering who did not hesitate to help me when needed.

I declare that I carried out this doctoral thesis independently, and only with the cited sources, literature and other professional sources.

In Prague, 22.02.2022

. . . . . .

Abstract

Fault detection and diagnostic are essential components of monitoring systems. Their main task is to increase safety and reliability by observing specific devices and distinguishing unusual behaviour. In recent decades, significant effort has been paid to developing fault detection methods for electromechanical actuators (EMA). One of the causes is the current trend in aviation, which aims to replace hydraulic, mechanical and pneumatic systems with electrical ones. However, implementing fault detection techniques may be associated with some issues, such as the need for intervention in the actuator by installing additional sensors, cabling, and supporting elements.

This thesis aims to eliminate some of these problems utilising the non-intrusive approach. Diagnostics performed by electrical measurements or Non-intrusive Load Monitoring (NILM) techniques bring benefits in the form of the absence of additional sensors, easy implementation and portability, lowering weight, costs, and complexity. In order to use this approach, it is first necessary to analyse the possibilities of its application in the EMAs, design and implement methods for fault detection and conduct adequate testing.

The proposed thesis is focused on fault detection methods for an EMA with a brushed DC motor. The jam and winding short faults as the most prominent EMA faults are considered. The fault detection is based on evaluating the properties of the motor current, taking into account the basic electromechanical parameters of EMA. The main advantages of the presented approach are utilising a commonly accessible measured quantity, easy applicability, and the ability to detect faults under varying operation modes of EMA, including changes of speed, load, or movement profiles. The proposed methods have been evaluated on the custom testing system. The results have proven the performance of the proposed approach to detect faults under varying operating conditions that could occur when used in industrial applications.

Keywords: Electro-mechanical Actuator (EMA), Fault Detection and Diagnostics (FDD), jam fault, winding short fault

Abstrakt

Detekce a diagnostika závad jsou důležitými prvky monitorovacích systémů. Jejich hlavním úkolem je zvýšit bezpečnost a spolehlivost sledovaného zařízení a včasně vyhodnotit jeho neobvyklé chování. V posledních desetiletích bylo věnováno značné úsilí vývoji metod pro detekci poruch u elektromechanických aktuátorů (EMA). Jedním z důvodů je současný trend v letectví, který si klade za cíl nahradit hydraulické, mechanické a pneumatické systémy elektrickými. Implementace technik pro detekci závad bývá spojována s určitými problémy, jako je nutnost zasahovat do akčního členu kvůli instalaci přídavných senzorů, kabeláže a podpůrných prvků.

Tato teze si klade za cíl odstranit některé z těchto problémů pomocí neintruzivního přístupu. Diagnostika prováděná měřením elektrických veličin nebo technikami založenými na neintruzivním sledování zátěže (NILM) přináší výhody v podobě absence přídavných senzorů, snadné implementace a přenositelnosti a také snížení hmotnosti, nákladů a složitosti. Aby bylo možné tento přístup použít, je nejprve nutné analyzovat možnosti jeho aplikace na EMA, dále navrhnout a implementovat metody pro detekci závad a provést odpovídající testování.

Předložená teze je zaměřena na metody detekce poruch u EMA s kartáčovaným stejnosměrným motorem. Konkrétně se jedná o závažné poruchy v podobě zaseknutí aktuátoru a zkratu vnitřního vinutí motoru. Detekce poruch je založena na vyhodnocení vlastností proudu motoru s využitím základních elektromechanickým parametrům EMA. Hlavními výhodami metod je, že k detekci závad využívají pouze jednu snadno měřitelnou veličinu, jsou jednoduše aplikovatelné a schopné detekovat poruchy v různých provozních režimech EMA, zahrnujících náhlé změny rychlosti, zatížení nebo profilů pohybu. Navržené metody byly testovány a ověřovány na speciálně sestaveném testovacím systému. Výsledky prokázaly, že navrhovaný přístup je účinný při detekci závad, za různých provozních podmínek, které by mohly nastat při používání v průmyslových aplikacích.

Klíčová slova: Elektromechanický aktuátor (EMA), Detekce závad a diagnostika (FDD), závada zaseknutí, závada zkratu vinutí

Contents

List of Figures

List of Tables

Nomenclature

APU Auxiliary Power Unit

BDC Brushed DC

BLDC Brushless DC

COT Computed Order Technique

ECU Electronic Control Unit

EMA Electromechanical actuators

FDD Fault Detection and Diagnosis

FFT Fast Fourier transform

HVDC High Voltage DC

IGD Integrated Drive Generator

IRC Incremental Rotary enCoder

MEA More Electric Aircraft

NILM Non-intrusive Load Monitoring

PHM Prognostic Health Management/Monitoring

PPR Pulses Per Revolution

RMS Root Mean Square

RPM Revolutions Per Minute

RTD Resistance Temperature Detector

TTL Transistor-Transistor-Logic

Chapter 1

Introduction

1.1 Motivation

Fault detection and diagnostics (FDD) are key components of many monitoring systems. The main priorities of these systems are distinguishing symptoms of unusual behaviour, identifying failure and determining a type of failure and location where the failure has occurred.

Monitoring systems can be found in many areas of industry, and the aviation industry is one of them. Commercial aircraft are sophisticated machines composed of a vast number of components. Such a complex system has to be constantly monitored and regularly checked in order to ensure high reliability and safety. Since the price of electronic components and computer systems is decreasing, it is convenient to use additional hardware for system health monitoring. On the other hand, the increasing complexity of aircraft systems makes this task more difficult [5].

For several decades great effort has been devoted to designing systems for aircraft health monitoring. Commercial aviation organisations invested many funds in health monitoring technologies to reduce maintenance costs, increase reliability, and improve efficiency. The current trend in aviation is to apply more electronic systems instead of mechanical. This trend is based on the More Electric Aircraft (MEA) concept, which has been known for decades but has only been partly implemented in recent years with the latest generations of commercial aircraft. The main obstacles of innovations are, in particular, the gradual implementation of new technologies, their thorough testing and, most importantly, lengthy certification.

The fundamental idea of the MEA concept is to replace pneumatic, hydraulic and semi-mechanical systems with electrical ones. This innovation reduces the aircraft's weight, which leads to lower fuel consumption and emissions of air pollutant gases. Moreover, the MEA concept brings other advantages such as optimizing the aircraft performance and decreasing the operation and maintenance costs [14].

The aircraft systems are driven from the different sources of power. The architecture of conventional aircraft is displayed in Figure 1.1.

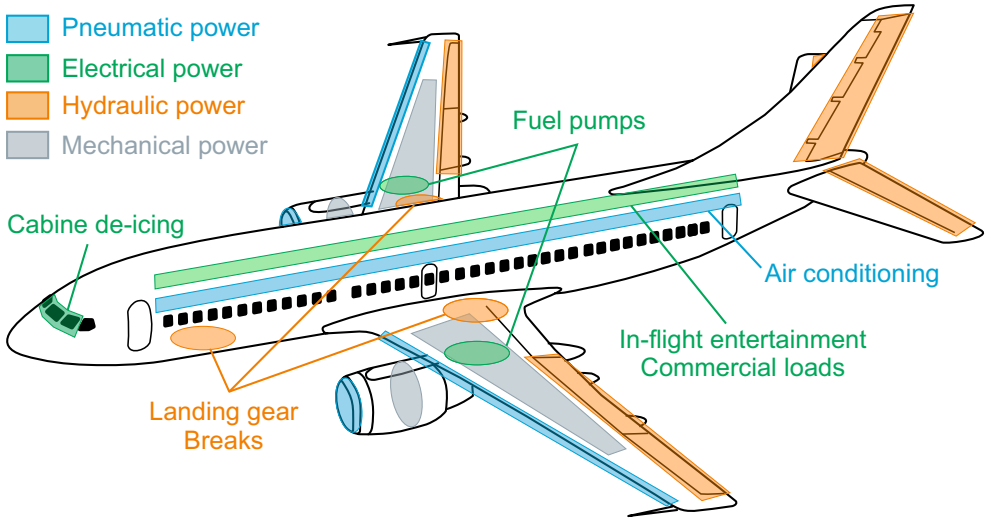

Figure 1.1: Power systems of conventional aircraft (according [13])

The pneumatic system uses high-pressure air, called bleed air, obtained from the engine's compressor. Controlled air leakage from the compressor produces enough energy for the pneumatic systems such as environmental control systems, the wing ice protection system, or engine startup, but it causes a decrease in the engine's efficiency.

The electrical grid of the aircraft is powered by several sources of electric energy. The primary energy sources are electric generators placed on each main engine. Another source is the auxiliary power unit (APU) that provides electric energy before the main engines are turned on. APU is started by the electric engine powered by batteries, and some aircraft are equipped with the ram air turbine, which is usually used in an emergency. The electrical system provides energy for commercial loads, avionics systems or eventually for weapon systems. The electric grid of commercial aircraft is usually composed of 115 V 400 Hz AC and 24 V and 28V DC power sources. According to [12], the gradual transition to the ±270 (HVDC, high voltage DC) is expected in the future because it should bring many benefits. The hydraulic system is used for the flight control actuators and landing gear, and it is powered by the mechanical system. The mechanical system uses mechanical power extracted from the engines by a shaft. This power drives hydraulic or fuel pumps and electric generators directly from the engine gearbox. The leading goal for the MEA is to remove the hydraulic and pneumatic system and reduce the mechanical system as much as possible. The hydraulic and pneumatic systems have o lot of common drawbacks. Both systems are costly, large, heavy and prone to leakage and contamination problems. Their replacement by electric engines and actuators would increase aircraft reliability, decrease weight, installation and operation costs and facilitate maintenance. Moreover, the electric system is easier to control and monitor. On the other hand, the MEA concept brings many challenges in areas of power generation and handling, power distribution, reliability and fault tolerance [13], [14].

Over the last few decades, there have been fundamental changes in the development of

new aircraft. Some parts of subsystems have been significantly reduced or even directly replaced by electrical systems. For instance, the Boeing 787 utilises electric-driven compressors for conditioning and pressurising the cabin instead of using bleed air taken from the engine compressor. Another change is eliminating an integrated drive generator (IGD) in some types of aircraft. IGD's shaft delivers constant speed despite the varying speed of a jet engine; therefore, it can provide constant voltage and frequency. Instead, Airbus A380, A350 and Boeing 787 use a more efficient generator coupled directly to a jet engine that provides a constant voltage with a variable frequency [22].

Bleedless aircraft is the aircraft type that does not use the bleed air from the main engine. The 787 No-Bleed system architecture, presented by Boeing, is currently the closest approach to the MEA concept. Boeing replaced most of the pneumatic systems with electrical to reach greater efficiency. Predicted savings of the fuel are about 3% [4]. No-Bleed architecture is significantly different from traditional aircraft's architecture is shown in Figure 1.1.

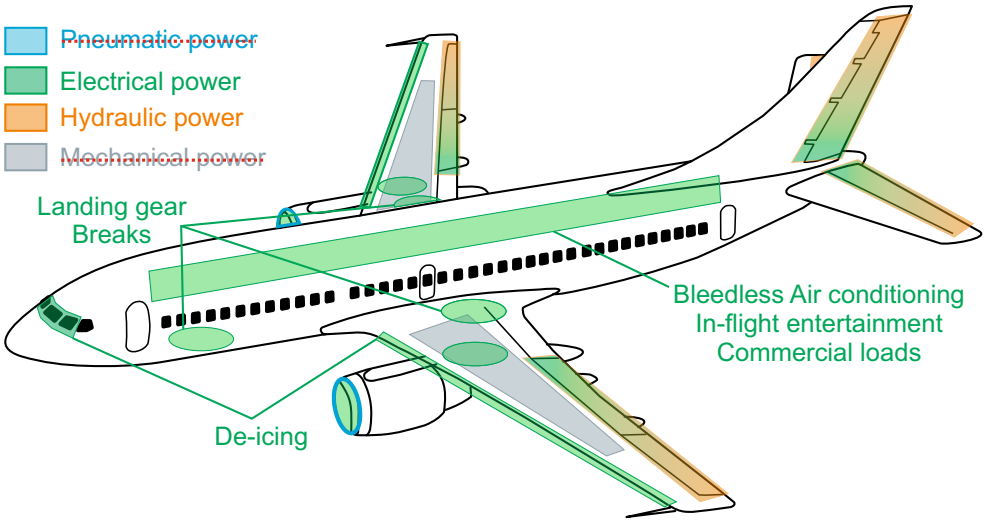

Figure 1.2: 787 No-Bleed systems architecture (according [13])

The pneumatic system was substantially reduced. The bleed air is used only for engine cowl ice protection and pressurization of hydraulic reservoirs, but the rest of the pneumatic system was replaced with electrical systems. The engines provide more electric power via shaft-driven generators. The APU now generates only the electric power, distributed to the engine generators that can also work as synchronous starting motors.

The hydraulic system comprises three independent systems - left, centre and right. These systems are usually driven by the engine-driven pumps mounted on the engine gearbox. In the No-Bleed architecture, the engine-driven pumps of the centre section were replaced with two powerful electric-motor-driven hydraulic pumps. This solution enables the aircraft to use hydraulic components which are smaller and lighter.

The environmental control system was significantly modified. Electrically driven compressors are used for cabin pressurisation since the main engines do not provide high-

pressure air. This concept is way more effective than the traditional bleed system because it does not require pre-coolers and modulating valves.

The no-bleed architecture does not use hot bleed air to de-icing the wing leading edge. The anti-icing and de-icing function is achieved by an electro-thermal ice protection scheme. This scheme brings higher efficiency because no excess energy is exhausted. Moreover, aeroplane drag and community noise are improved because exhaust holes are no longer needed.

The concept of a bleedless aircraft brings many advantages such as improved fuel consumption due to a more efficient secondary power extraction, lower maintenance costs due to removal of the bleed system, lower weight due to elimination of pneumatic system components and other subsystems and improved aircraft reliability.

Another possible improvement lies in the electrification of hydraulic systems. In traditional aircraft, hydraulic systems drive or move mechanical components such as primary and secondary control surfaces, braking, landing gear and many others. These systems are usually driven by mechanical actuators, but the current trend is to replace them with electromechanical actuators (EMAs) or electro-hydraulic actuators (EHAs). Electrically driven actuators' employment instead of hydraulic actuation can decrease maintenance costs, reduce weight, and increase system efficiency [8], [22].

The More Electric Aircraft concept brings a lot of innovative elements that are key to the future of the aviation industry. The application of elements from this concept should bring many benefits such as increased safety and reliability and reduced components, weight and operating and maintenance costs. However, all new technologies must first be thoroughly tested and certified. This process is time-consuming and costly, which is also why individual technologies are gradually being introduced over a long time.

1.2 Problem Statement

Electromechanical actuators are a great way to meet the goals of the MEA concept. Compared to the hydraulic systems they should replace, their most significant advantages are low weight, reliability, low maintenance, scalability, easy to implement self-test and monitoring and high efficiency. In addition to replacing hydraulic systems, they can be used in low-power applications thanks to their easy controllability and compact designs.

The most desired objective is to use EMAs to control primary and secondary flight surfaces. However, this promising and ambitious goal has not yet been fully met. In order to prove the long term reliability of EMA, complex testing of partial components is needed. Pros and cons and reasons why these solutions have not spread rapidly enough are explained in [32], [42]. Currently, EMAs are used on a smaller scale in some subsystems of commercial aircraft and dedicated experimental systems. For example, EMAs are used for the nose wheel steering system of F-16 [27], A380 and A350 utilise EMA technologies for thrust reverser application [23] or Boeing 787 using EMAs for breaking, spoiler actuation, and horizon stabiliser trim [27].

The involvement of EMAs is significant not only for aerospace but also for other industrial applications. The possibilities for EMA's employment in various systems and subsystems are considerable. They can be used in multiple transient or pulsed actuation functions such as door manipulation, extension/retraction, locks, steering, braking, opening and closing valves, positioning of flaps, fins and so on [9], [16], [32].

However, innovative systems such as EMA bring new challenges, especially in the area of safety and reliability. The are as well as any electromechanical device prone to failures. Undetected failures and degradations can have a negative effect on actuator operation, leading to an increase in maintenance and costs, and could be potentially dangerous, especially in safety-critical applications. Although EMA are widely used in industry, and their parameters are well known from the functional point of view, it is first necessary to examine various fault modes of their components [6]. In order to fulfil strict safety requirements, EMAs must be equipped with a sophisticated system of self-monitoring. A smart actuator should have integrated equipment to detect faults and degradations or prognostics and health management system [6], [8].

The main benefit of monitoring systems is that they can be used to observe the condition of the equipment and detect faults at an early stage of development. In addition, predictive algorithms can be implemented to estimate the remaining life of the actuator or to monitor the occurrence and development of degradation. Monitoring systems use combinations of information from various sources, such as data from sensor networks, inputs and outputs of the control unit or data based on system model simulations. The typical quantities used for EMA diagnostic are electric current, voltage, temperature, position, force, vibration or rotation angle, which are usually measured by sensors. These devices represent additive hardware that requires power supplies, takes space, complicates handling, and increases complexity and costs. In addition, installing some sensor types requires intervention in the actuator by adding mounting elements, cabling for power and data transmission, or equipment for signal conditioning, amplification, and processing. Such modifications can increase the weight, overall price or maintenance costs.

A non-intrusive monitoring approach is a great tool to eliminate some of the problems mentioned above. Diagnostics utilising electrical measurements or NILM-based (Non-intrusive Load Monitoring) techniques benefit from the absence of additional sensors, easy implementation and portability, low weight, costs, and complexity. As a result, there is no need to interfere with the actuator, and diagnostics can be performed at the level of the control power unit. Moreover, no additional wiring is needed because it is measured directly on the cables that supply EMA. Diagnosis based on these principles is the focus of this dissertation thesis.

Chapter 2

State-of-the-Art

2.1 Fault detection methods for EMA

Fault detection and diagnostic and condition monitoring are an integral part of machine diagnostics. Electromechanical actuators (EMA) are very well-tested devices. Although these are generally very reliable machines, their failure modes or the mechanisms that lead to their defects have not yet been adequately tested. One of the major problems is the great variety of possible mechanical arrangements. Actuators are usually assembled in various combinations using different electric drives, mechanical transmissions, or design solutions depending on the required application. AC and DC motors, such as brushed DC (BDC) or brushless DC (BLDC), induction AC, permanent magnet synchronous or stepper, are often used as electric drives. This variety also leads to a considerable range of parameters such as force, stroke length (in the case of linear actuators) or rotation angle (in the case of rotary actuators), movement speed, duty cycle or operating voltages and currents.

EMAs have become widespread in recent decades, and their gradual implementation into critical applications is beginning to be considered. First of all, however, it is necessary to sufficiently test them and develop methods for fault detection and systems for condition monitoring that helps to predict failures in time before they occur. EMA fault diagnosis poses an interesting research problem as it is composed of electrical, electronic, and mechanical subsystems, which results in intricate failure modes and effects [6]. In recent years, significant efforts have been made to develop similar systems and methods.

2.2 Review of methods

Fault detection, diagnosis and monitoring methods can be divided based on the used approach. Model-based approaches typically involve the creation of an accurate mathematical model to predict the outputs to a set of inputs for assessing health. The noted benefit of the model-based approach is that failure modes are traced back to model parameters to provide insight into fault diagnosis failure. The drawback of the model-based approach

is that models are often complex and must be validated. As such, the models are then dedicated to the specific application, and new models must be created and validated for each new application. Also, implementing this type of scheme in an EMA controller, for instance, would require a significant amount of processing capability when added to the standard control and management schemes typically employed for flight control actuators. Unlike model-based techniques, data-based approaches operate directly on signal data, using signal processing techniques and "black box" models to expose patterns/signatures in signal data that give insight into machine conditions [17].

This part of the thesis summarises scientific works dealing with the topic. The overview contains a description of the main ideas of individual research and the means and procedures by which they were achieved.

2.2.1 Model-based methods

The work described in [29] presents the model-based monitoring concept of a primary flight control system comprising two electromechanical actuators. The article includes a comprehensive description of all models of the actuation system such as permanent magnet synchronous motor with three-phase inverter, reduction stage - gearbox, roller screw, actuation system-aileron coupling, Stribeck's friction, backslash, and non-linear servo-control loop. The study examines relationships among process variables that indicate the presence of a specific fault and suggests a few monitoring methods. The goal of monitoring methods is the detection and isolation of a fault. Proposed methods are primarily based on the evaluation of discrepancy between the position being commanded and the actual position of some part of the system or the difference between actual positions of two-part of the system. The evaluation processes consider the information from the control systems, sensors, time dependencies of specific actions and results of voting algorithms of redundant parts of the system.

The authors of the study used the model of the system for the definition of detection thresholds for monitoring functions. The signal and time thresholds are obtained based on uncertainty and reachability analysis. Experimental and virtual verification is employed to test the efficiency of the developed monitoring functions. The faults that do not require hardware intrusion are experimentally verified on the test rig, and faults that cannot be non-intrusively emulated were verified through simulation. Four critical faults are examined in the study: loss of one linear variable differential transformer (LVDT) signal, mechanical blocking in one actuator, single electrical power loss, and loss of one load cell signal.

The research described in [35] demonstrates the model-based Prognostic Health Management (PHM) algorithm for the identification of the mechanical transmission freeplay (backlash) of electromechanical flight actuators. The proposed algorithm uses prognostic models generated from a high-fidelity model of the actuator, in which increasing values of freeplay are imposed. The functionality is demonstrated on a system which is composed of a 3-phase brushless DC motor, a mechanical transmission with a spur reduction gearbox, a

four-bar linkage connecting the EMA output lever to the flight control, a power electronics bridge with six MOSFET driven by Space-Vector PWM technique (i.e. via Clark transforms) and sensors such as Rotary Variable Differential Transformer (RVDT), a resolver measuring the motor shaft rotation, three current sensors. The system model developed in Matlab-Simulink includes simulations of 3-phase brushless DC motor dynamics, mechanical transmission vibrational dynamics, mechanical nonlinearities (efficiency loss, sliding friction, and four-bar linkage kinematics), freeplay, sensors' dynamics and errors and digital signal processing of the closed-loop controls. The basic idea of the proposed PHM is that freeplay in flight control electromechanical actuators (EMAa) implies the onset of limit cycle oscillations, with amplitude and frequency that depends on the freeplay size. The PHM algorithm is designed to be used during maintenance. It collects the time histories of the actuator sensors during position tracking tests capable of inducing freeplay-related limit cycles, and operates a signals' treatment (Fast Fourier Transform), normalisation, amplification, filtering) aiming to valorise the limit cycle content concerning high-frequency disturbances and low-frequency dynamics. The Maintenance Built-In Test (MBIT) has been simulated on each prognostic model to create a PHM database. The amplitude and the frequency of the measured limit cycle oscillation are then compared with the database by generating a freeplay estimation and a remaining useful life prediction. The algorithm uses (FFT) and postprocessing to process data from sensors (resolver, RVDT, currents). The data are analysed in the expected frequency range for the limit cycle onset (from 0.3 to 1 Hz), by searching the peak of the distribution. The measured amplitude and frequency are compared with the PHM database. The accuracy of the proposed PHM algorithm has been characterised by repeating the simulation of the MBIT with different values of EMA freeplay, by evaluating the effects of model uncertainties on the PHM outputs.

The follow-up research [21] and [34] deals with stress factors affecting the lifespan of insulation materials of devices such s EMA motors in aerospace applications. The effect of electrical faults of stator or rotor winding are examined, and four significant sources of stress in winding insulation are described [6]. The sources of stress are summarized into groups as electrical: voltage, transients and frequency affecting adjacent turns, ambient: pressure and humidity, thermal: oxidation chemical reaction caused by a change of temperature and thermo-mechanical: thermal cycling of coils.

The multi-stress lifetime model of the winding insulation of electrical machines is proposed [7]. The ageing process is described as repeatedly breaking the chemical and physical bonds between the atoms of the substance that are reorganized and reformed in new configurations. Based on this definition, two models are presented: the statistical model comprising thermal and electrical stress and the physical model. The authors further investigate the hybrid approach, which includes the Crines model and the Lewis model and the procedure of multi-factor modelling, which combines previous life models.

The experiment which investigates the dependency between the air pressure and is partial discharge is presented. The results showed that partial discharge inception voltage decreases when the atmospheric pressure decreases.

The work described in [31] deals with the development and the performance characterisation of two health-monitoring algorithms for electromechanical flight control actuators. Both algorithms are based on dynamic position predictors and detect a malfunction when the actual feedback deviates from the prediction for a predefined threshold. The tested electromechanical actuator system is composed of an actuator control unit, a 3-phase permanent magnet synchronous motor with sinusoidal modulation, and a mechanical transmission made of a two-stage gearbox and a screw jack. The sensor architecture contains a supply voltage sensor, temperature sensor, six current sensors, three voltage sensors, a resolver, and two LVDT transducers.

Both proposed position tracking monitors (PTM) use time-discrete dynamic predictors estimating the electromechanical actuator System (EMAS) position. The inputs of the PTM have been limited to position demand, LVDT sensor for monitoring loop position feedback and voltage supply level. The first-order and second-order position predictors are presented. The fault-detector logic (FLD) uses the normalised output from predictors and evaluates the fault using the decision tree and fault counters.

The two versions of the PTM have been compared in terms of fault detection capabilities by using a high-fidelity model of the EMAS, which is stimulated by the time history of a light military jet trainer elevator during severe pull-up/pulldown manoeuvres in normal conditions and with different types of faults (motor coil faults, motor magnet degradation, voltage supply decrease). The two algorithms show similar performances for false alarms rejection, detection of motor coil faults and abrupt voltage decrease, but only the algorithm with a more accurate speed predictor can detect magnet degradation phenomena.

In [28], the researchers present the approach of how to model a three-phase brushless DC motor (BLDCM) for an electromechanical actuator. The Simulink model is based on the voltage equation, torque equation and motion equation of the BLDCM and simplifying assumptions. The work is primarily focused on winding defects since it is considered the most susceptible component of the motor. The faults of EMA such as phase turnoff, phase short fault or inverter short are analysed and simulated.

In [33], fault detection in airliner electromechanical actuators via hybrid particle filtering has been introduced. In work, the test rig of the actuator of primary flight surfaces of a wide-body airliner has been designed.

The test rig has been used to simulate fault scenarios related to sphere damage, particularly steel ball spalling. Data were collected from the test bench, and a model was identified for each of the four-fault conditions. The OTPF (Observation and Transition Particle Filter) and the EKF (Extended Kalman Filter) were used to compare non-linear filtering techniques regarding fault detection capability.

Both techniques were evaluated using the data from four different models. They provided promising results even when Gaussian noise was added; however, when a non-gaussian noise was introduced, the OTPF method clearly won. Experiments suggest that the particle filter algorithm can benefit non-standard disturbances and strong non-

linearities.

The research [7] describes a design of an experimental test stand utilising electromechanical actuator. The test stand was used to develop the model-based PHM of aircraft EMA systems using a hybrid (virtual sensor) approach.

The model-based approach to PHM applies physical modelling and advanced parametric identification techniques. The approach employs a dynamic mathematical model of the system that is directly tied to the physical processes that drive the component's health. The model is identified by simulations with the expected responses. The difference between the simulated and actual response is used to estimate system parameters (e.g., efficiency, friction factors, etc.). The model is then used for simulations of faults. These faults were injected as gain, bias, and/or noise blocks on various parameters and signals within the model. The system's response to various simulated faults, such as loss of power to the motor, winding short and position sensor fault, was analysed and verified. Fault diagnoses for HPM were achieved by deriving features from the actuator signals and correlating these features to fault severity levels. Also, the simulation of all three faults simultaneously was performed. The derived features can reliably separate these faults for the most part, with brief inaccuracies manifesting when the level of the simulated fault abruptly changes.

2.2.2 Data-based methods

The researchers in [6] present an analysis of critical fault modes for EMAs and describe an approach to detecting them using artificial neural networks.

The most significant contribution of this study is a comprehensive fault analysis of electromechanical actuators. This analysis is often cited in other research and serves as a basis for assessing defects from the frequency of occurrence and criticality. The EMA faults are divided into four general categories: sensor, mechanical or structural, motor, and power or electrical. Failure Modes and Criticality Analysis (FMECA) references, literature reviews, and accessible industry experiences have been utilized to create a list of failures. A subset of faults (return channel jam, spalling, sensor bias, sensor drift, and sensor scaling) was then selected for a more detailed study.

Experiments on selected faults have been performed using an electromechanical actuator test stand. The data (temperature and vibrations) obtained in these experiments were used to test the neural network-based diagnostics system. The system results are described using the percentage of false positive, false negative and misclassification rates. The authors admit that if there are significant changes in load characteristics, which result in a difference in baseline conditions, a classifier that is not appropriately trained cannot work correctly under these conditions.

The research described in [17] investigates a data-driven approach for condition monitoring consisting of feature extraction and fault classification. The proposed approach is based on assigning a class that relates to the condition of the EMA based on the sensor

measurement. The feature extraction aims to expose faults that produce signatures in the frequency domain that are synchronous with the motor position.

This method is composed of several steps. Sampled data of measured signals are resampled to the position domain. Position domain is more suitable for EMA because fault signatures are periodic with the motor position. Resampled data are then transformed into the frequency domain by computing the power spectral density (PSD). The power spectral density data are filtered, converted to energy bins, and reduced by a feature space transformation process.

The health status is classified based on the Bayesian classification, which has been trained on known data. The method is demonstrated on simulated data and a real experiment. It utilises vibrations from an accelerometer and electric current measured as input to detect the ball bearing defect (BBD) and ball screw defect (BSD). The ball bearing defect can be detected using both signals; however, the measured current was not efficient in the case of the ball screw defect. The authors concluded that vibration measurements are more suitable for fault detection based on experiments.

The research in [37] explores data-based monitoring methods that can be applied to different types of EMA. The methods are based on the automated extraction and the analysis of signal features such as steady value, overshoot, settling time, or presence of unexpected peaks that characterise the system's dynamic behaviour.

The study is focused on feature extraction, primarily from the current and position measurement. The Principal Component Analysis has been used to decrease data redundancy.

The instrumented test rig has been built to evaluate the performance of the proposed algorithm. The test rig is composed of two EMAs connected to the linear guides. One actuator serves as a load to the tested actuator.

The data has been collected under nominal operating conditions (absence of faults) and after introducing the typical faults such as lack of lubrication, spalling and backlash. Two presented methods collect and evaluate features such as steady value, overshoot, settling time, unexpected peaks and standard deviation of a measured entity. The algorithm can detect the faults introduced, although detection in the early stages of degradation was not always possible.

The research presented in [26] deals with hybrid vibration-based fault detection and classification for EMAs. The paper investigates a technique for the early detection of latent faults in EMA ballscrews. The two faults considered in the study are a partial jam and a spall (i.e. metal flaking) in the actuator ballscrew mechanism.

The concept of using ballscrew kinematics for estimating the health condition of an actuator is based on the characterization of the interaction between the balls in the ballscrew mechanism and the fault region.

The Computed Order Technique (COT) has been used to transform transient vibrations measured during variable speed motion into ordered vibrations.

Vibration signatures are characterized by their frequencies. The ball-passing frequency concerning a fixed point on the nut, the ball passing frequency concerning a point fixed on the screw and amplitudes of these frequencies are used for fault classification. The theoretical concept has been tested and evaluated on the data from the real test stand composed of three different actuators: one nominal, one injected with faults, and the third providing dynamic load.

The health monitoring method of the electromechanical actuator using the Σ feature has been proposed in [36]. The method is based on evaluating the root mean square (RMS) of three phases currents. The method has been focused on an electromechanical actuator specifically designed for aircraft, and it is equipped with an Electronic Control Unit (ECU). The unit is directly assembled on the actuator, where all the control systems (current, speed and position control) are implemented. The ECU operates through a 28 Vdc power supply and controls the three-phase electric motor.

Many sinusoidal position cycles with an external load greater than the nominal one have been performed. During experiments, the fault was injected by gradually eliminating the lubricant. The proposed health monitoring method has been applied to the data measured and evaluated results. The Σ feature proved to be a valuable parameter for the health monitoring method, which uses historical data.

2.3 Summary

Methods for condition monitoring, diagnostic and detection of faults and degradation can be divided into two groups.

Model-based approaches require creating an accurate mathematical model that simulates a given device. The advantage is that it is possible to monitor individual states of the model, which can be used for diagnostic. The disadvantages are that the accuracy of the simulations depends on the specific implementation of the model and also that the simulations can be computationally intensive. In addition, such models are designed for only one application, and if they are to be used elsewhere, the model must be modified, re-validated and device parameters re-identified.

In contrast, data-based approaches use sensor networks that provide data for diagnostic purposes. The system is viewed as a black box, and only its output parameters are monitored. The advantages of this approach are better portability and usability in other applications. The disadvantage is the need for interventions in the monitored equipment by installing sensors, cabling, power supplies, and units for data collection, processing and evaluation.

Methods for fault detection and diagnosis are important elements that can increase safety reliability and help reduce operating and maintenance costs. However, their implementation is associated with many problems. The fault detection approaches described in section 2.2 often rely on systems that require additional elements, including power supplies, cabling, additional sensors or computing and signal processing units for proper operation.

These components not only increase weight, complexity and price but also complicate the installation and handling. In addition, the implementation of such a system requires modifications and interventions in the actuator in order to attach additional elements and cabling.

Chapter 3

Aims of the doctoral thesis

This work aims to propose diagnostic methods for electromechanical actuators. The main goal is to eliminate some problems of conventional methods described in section 2.3, such as the need for intervention in the actuator by installing additional sensors, cabling, and supporting elements. The presented solution lies in the use of a non-intrusive approach. The thesis is focused on the diagnostics of electromechanical actuators with brush DC motors that are still often used in industry due to their low price and easy controllability. They are usually utilised in low power applications for positioning valves, doors, dampers, or locks [9], [16].

3.1 Specific aims of doctoral thesis

This thesis aims to design, test and evaluate methods for detection of faults and degradations in EMA using a non-intrusive approach. To achieve this goal, it is necessary to accomplish several steps:

- **Analysis of specific EMA faults:** Linear electromechanical actuators typically consist of a motor, gearbox, lead screw, movable rod and body. Each of these components is prone to a different type of failure with a different probability of occurrence. The aim is to analyse the individual components in order to clarify the mechanisms that lead to failures or degradations. This analysis is used to select defects that are monitorable using a non-intrusive approach.

- **Design of fault detection methods:** The main goal is to design methods for EMA fault detection with a brushed DC motor. Emphasis is placed on a non-intrusive approach, easy portability, simple implementation and low computational complexity.

- **Design of testing system for EMA:** To perform experiments with electromechanical actuators, creating an automated test system is necessary. Its main task is to

automatically conduct experiments according to predefined parameters and collect and process the tested actuator's data.

- **Testing of proposed methods:** The proposed solutions must be comprehensively tested to verify fault detection abilities in various operating conditions, including variable speeds and loads during different motion profiles.
- **Evaluation of method properties:** The reliability and durability of the presented methods must be evaluated. Experiments are needed to help identify situations with risks of failure and propose a procedure to minimize these risks.

Chapter 4

Analysis of EMA faults

4.1 Construction of EMA

The linear electromechanical actuator is an actuator that converts the rotary motion of a motor into a linear displacement. A typical actuator with a DC motor is shown in the Figure 4.1.

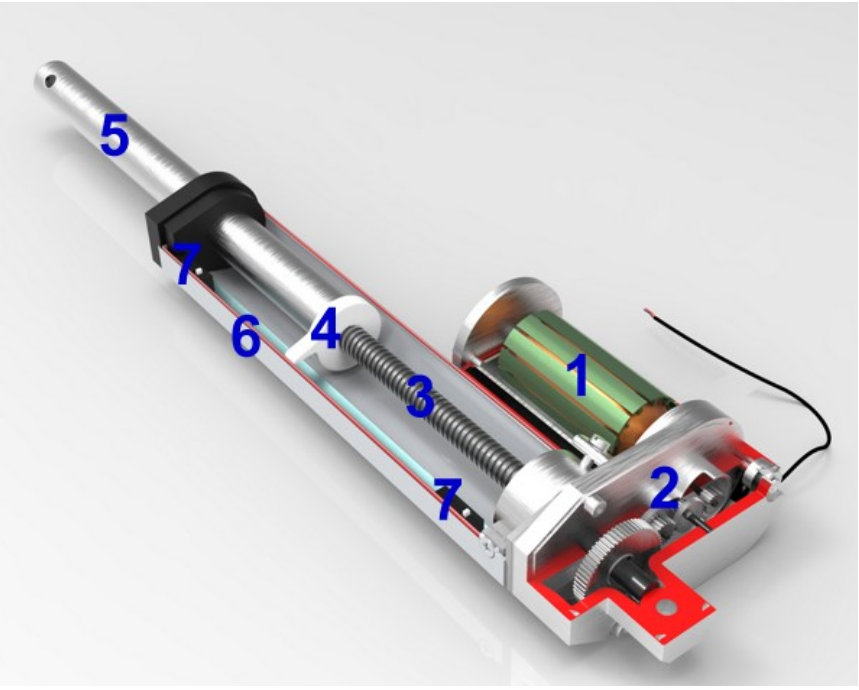

Figure 4.1: Linear electromechanical actuator with brushed DC motor [source: www.firgelliauto.com], 1 - DC motor, 2 - Gearing, 3 - Lead-scew, 4 - Nut, 5 - Rod, 6 - Housing, 7 - Limit switches

The EMA consists of a brushed DC motor attached to the gearbox. The gearbox with reducing gears drives the lead-screw on which the nut moves. The nut is equipped with a pin that slides in the housing groove and prevents the nut from turning. A lifting rod transmitting the linear movement of the actuator is attached to the nut. The actuator can be equipped with limit switches triggered when the nut is in one of the extreme positions. The control unit can use the provided information to stop the movement in a given direction in order not to damage the actuator.

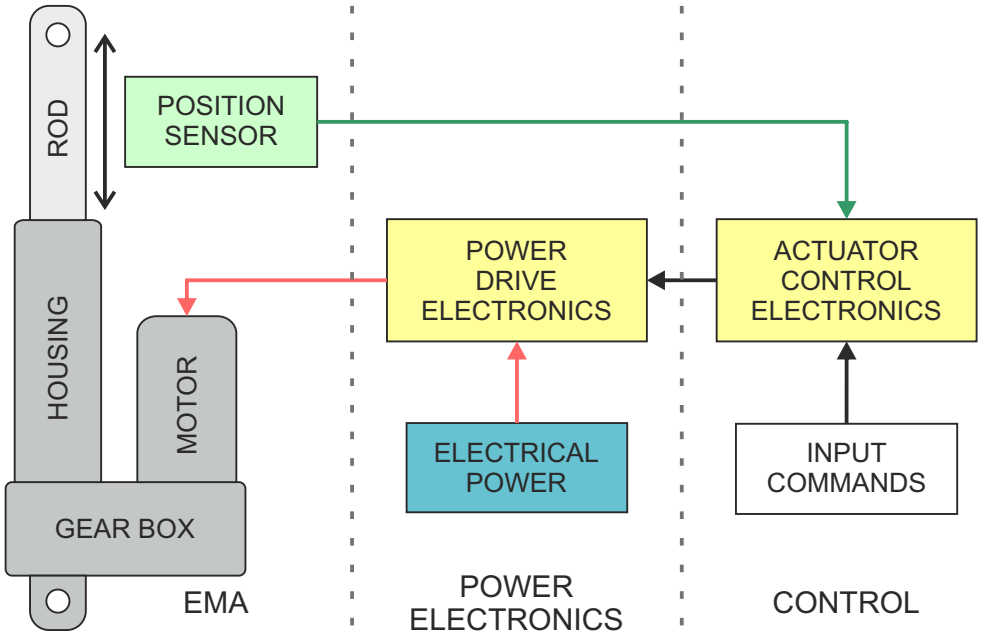

Figure 4.2: Block layout of EMA

The block diagram of the electromechanical actuator with control elements is shown in Figure 4.2. The actuator itself consists of a motor, a gearbox, a housing, a lifting rod and a position sensor. The gearbox is typically consisted of reducing transmission on the leading-screw shaft, either by gears or a belt drive. The actuator is controlled by control electronics, consisting of power drive electronics and an actuator control electronics using information from the feedback sensor. The controller compares the position data with the required input parameters and creates a control action for the power drive electronics. The power drive electronics composed by the H-bridge then supplies the motor.

4.2 Standard EMA blocks

4.2.1 Motor

The motor of the electromechanical actuator produces a rotary motion, which is then converted to linear, most often employing gears and a screw rod. The classic brushed DC motor consists of a stator, rotor, commutator, supply cables and cover. Motor faults are among the most common actuator faults [6]. The leading cause is the mechanical stress when working at high speeds, which leads to considerable heating in their housing. The preview of the open engine is in the image 4.3.

Figure 4.3: Opened motor housing

4.2.1.1 Rotor

The rotor is a rotating part of the motor, consisting of a shaft, coils and a commutator. The rotor is one of the most mechanically stressed parts of the engine. Rotor faults are primarily associated with coil winding [21]. These defects are mainly caused by the thermal stress of the winding. Typical faults include winding faults (short circuit and open winding, which are closely examined in section 5.1.3), commutator related faults, and rotor imbalance.

Commutator The commutator is a mechanical rotary rectifier that switches the current to the stator coils. It is located on the motor rotor and is supported by graphite brushes

located on the stator. High currents pass through the commutator, which makes it a highly stressed part of the DC motor. The operation of the commutator is accompanied by unwanted sparking caused by air gaps between the commutator blades and the graphite brushes. During operation, there is gradual wear of both the commutator and graphite brushes, which is the most common source of failure of these machines.

The commutators exhibit defects such as blackening or burning of the slats (commutator segments), copper gathering, vibration, corrosion or breakage of the slats. Common causes of these faults are overloading, imperfect contact between the commutator and the brush, uneven brush pressure, brush jams in the dirt grooves or loose commutator blades.

Commutator faults can cause reduced motor power, increased vibration, sparking, or overheating of the motor.

Imbalance Balancing issues are discussed in [18]. Motor imbalance is caused by uneven mass distribution in the rotor. The centrifugal force caused by the unbalanced mass is transmitted to the bearings at each revolution and results in motor vibrations that negatively affect the support structures. As the speed increases, so does the vibration generated by the centrifugal force, as the centrifugal force increases with the square of the speed.

The most common source of inadequate balance is poor production processes. In addition, imbalances can also occur as a result of operation over time. Thermal loading during operation can result in an uneven expansion of the material and thus a shift in the centre axis of inertia, which also contributes to poor balance.

Engine balance or vibration can be monitored using accelerometers. Imbalance detection could be based on monitoring the increase in vibration associated with engine rotation during nominal operation.

4.2.1.2 Stator

The stator of a brushed DC motor with permanent magnets consists of a housing in which the magnets and commutator brushes are mounted. Thanks to the simple concept of this type of engine, it is not an overloaded part of the engine. There is a risk of malfunction if one of the permanent magnets is released or shifted. In such a case, the stator magnetic field would be disturbed, or the neutral plane would shift. Disruption of the stator magnetic field reduces motor efficiency, a shift of the neutral axis to higher commutator sparking, and greater heating.

As the operating temperature increases, the magnetic induction decreases, which changes the electromagnetic constant of the motor. At higher temperatures, irreversible changes may occur depending on the type of magnetic material, and after exceeding the Curie point, magnetisation is lost [3]. The maximum operating temperature is 300 °C in the case of SmCo and 150 °C in the case of NdFeB magnets.

4.2.2 Connectors and cables

The supply cables are usually firmly connected to the control unit, either by soldering or using connectors. They can be mechanically damaged if they are exposed to vibration, mechanical stress or excessive temperatures. These phenomena can lead to disconnection of the connectors or, in the case of cables, to a short circuit, which will cause the actuator to lose functionality. Excessive stress can also occur if the current-carrying capacity is exceeded. In this case, temperatures will rise, which could damage the cable insulation or damage the contacts. Poor contact is characterised by increased transient resistance, limiting the current to the actuator and thus reducing its performance.

4.2.3 Mechanical transmission

The mechanical transmission between the motor and the actuator leading-screw consists of a set of reducing gears in a gearbox. Diagnosis of gearbox problems could be based on vibration, temperature, or acoustic emission measurements. The gearbox is in the picture 4.4.

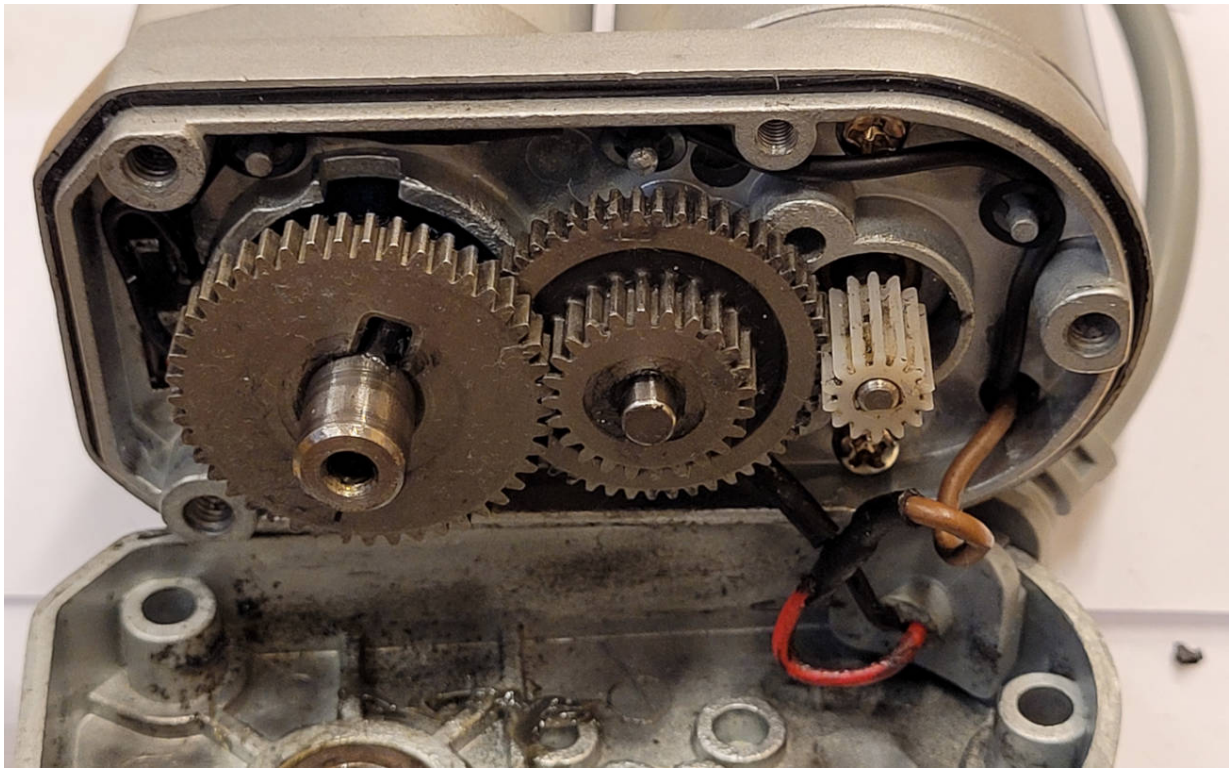

Figure 4.4: Opened EMA gearbox

4.2.3.1 Gears

Gear transmissions are prone to defects associated with tooth surface damage and tooth breakage damage. The surface of the teeth can be damaged by abrasive wear (particles in the lubrication), adhesive wear (seizing at the head of the teeth), permanent deformation (plastic, pitting, corrugation, grooving, burrs) or peeling of flat parts. Furthermore, surface fatigue of the teeth is caused by the propagation of subsurface cracks arising from cyclic surface stress and manifests itself as pitting. Damage due to tooth breakage is caused by a sudden overload above the strength limit or a manufacturing failure of the material. Another cause may be fatigue fracture of the teeth caused by cyclic overloading above the material's fatigue or time strength limit.

4.2.3.2 Bearings

The rotating parts of the actuator use plain bearings, both at the actuator bolt and at the gears. Plain bearings suffer from interrelated problems associated, in particular with lubrication, backlash, stability and wear. Their issues are described in detail in [10]. Typical plain bearing failures are dry friction problems, oil instability, grooving (circumferential grooves from abrasive particles/dirt), fatigue cracks in the composition (excessive dynamic stress), corrosion (for lead compositions due to acidic oxidising components of the oil), cavitation vibrations, and erosive wear or pitting from electric shocks (ungrounded rotor). These faults, which lead to bearing instability, are most often manifested by heating, vibration and deterioration of rotation. The resulting instability of the bearing then represents a state in which self-excited vibrations occur due to various circumstances.

4.2.4 Leading-screw and nut

The actuator leading-screw, which is attached to the gearbox's output, consists of a threaded metal rod and, together with the movable nut, serves to convert the rotary motion into a linear one. The preview of the matrix in the open actuator is in the picture 4.5. 4.5.

The mechanical defects arising in these two components are similar in nature and interact. Defects such as insufficient lubrication, spalling or backlash are typical examples [37].

Insufficient or poor lubrication leads to excessive friction and increases temperatures at the point of contact of these components and their subsequent wear. In a critical case, a complete jam may occur, and thus the actuator may lose functionality.

If the materials wear out, small pieces may start to peel off (crumbling), further degrading their surface. The result is permanent damage, which leads to a deterioration in the actuator's smoothness of movement and performance.

The backlash caused by the wear of these two components results in kickbacks. If they occur, the smooth running of the actuator is disturbed, which is loaded by excessive shocks. These faults manifest as a continuous or sudden increase in the actuator load. Their

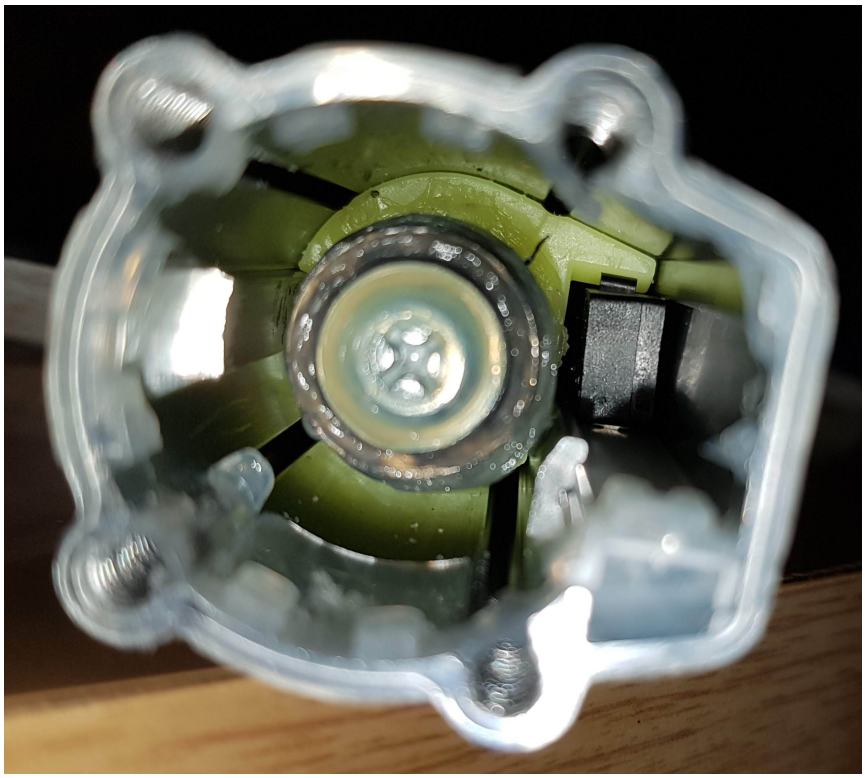

Figure 4.5: Nut (yellow-green) in the actuator housing

detection could be based on measuring the temperature of those components, monitoring the trend of increasing peaks in the current taken or monitoring increased vibrations.

4.2.5 Actuator body/housing

The actuator housing is a durable component, which can be expected to have a low defect rate. Defects of housing are most often associated with poor design, poor production process or used material. Housing main task is to connect the entire actuator structure and prevent dirt from entering.

4.2.6 Power supply

The power supply must be powerful enough to provide the necessary power. Inrush currents at motor run-up can be several times higher than the maximum continuous current at full load. The power supply must therefore be able to cover these spikes without voltage drop. Faults of power supplies are usually caused by the degradation of loaded components. The most critical components of switching power supplies are electrolytic capacitors, power MOSFETs and diodes [15].

The main cause of degradation of electrolytic capacitors is the evaporation/drying of the electrolyte, which leads to an increase in series resistance and a decrease in capacity. At constant temperature, there is a linear loss of capacity over time and an exponential increase in the series resistance described in equations 4.1 and 4.2.

$$ESR(t) = A_1 e^{B_1 t} \tag{4.1}$$

$$C(t) = A_2 + B_2 t \tag{4.2}$$

where A_1, A_2, B_1, B_1 are coefficients of specific capacitors and t is time. Fast Schottky diodes, which are used in switched power supplies, degrade by loading with high currents, voltages and temperatures on the contact interface of metal and semiconductor. The degradation results in a significant increase in current in the reverse direction. This process can be described using the Arrhenius model as

$$\frac{\Delta I_R}{I_R} = A e^{(-\frac{Q}{kT})t} \tag{4.3}$$

where I_R is reverse leakage current, A the constant for a particular diode, Q the activation energy, k the Boltzmann constant and T the absolute temperature.

Degradation of power MOSFETs is caused by mechanisms such as hot carrier injection (HCI), bias temperature instability (BTI), time-dependent dielectric breakdown (TDDB) or metal electro-migration. MOSFETs are electrically and thermally stressed, which can be described by the model in the equation.

$$\frac{\Delta X_R}{X} = A e^{V^m} e^{(-\frac{Q}{kT})t} \tag{4.4}$$

where X are the temperature sensitive electrical parameters, A is the transistor coefficient, V is the voltage, m is the constant, Q is the activation energy, k is the Boltzmann constant and T is the absolute temperature.

4.2.7 Control unit

The control unit consists of a power H-bridge powered by the power supply and driven by signals from the controller. The H-bridge is an integrated semiconductor device that must sufficiently handle the power spikes of the actuator. If the bridge is overloaded, one of the power transistors could be damaged due to the degradations described in the 4.2.6 chapter. The damaged transistor ceases to be controllable, and it is stuck in a close or open state. If one transistor is permanently open, the actuator's controllability is lost. The fault manifests in zero current when running in one direction. When multiple transistors are open, there may be a complete loss of control. If the damaged transistor is permanently close, when the second transistor on the same branch is switched on, the source is loaded with very little resistance (typically tens to hundreds of $m\Omega$), and the bridge behaves like

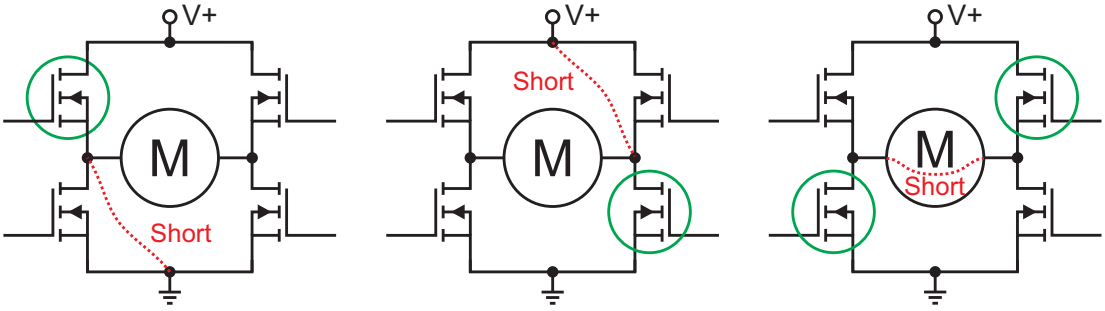

Figure 4.6: Dangerous short-circuits of the H-bridge. Green circle indicates a closed transistor

an electrical short circuit (shown in the Figure 4.6). This condition is hazardous because it exposes the circuit to high currents. Faults in the switching transistors can be detected by measuring the direction and magnitude of the current flowing through the bridge and comparing these ranks with the control signals. Problems can also occur in the case of poor control when two transistors on the same branch are closed at the same time. Modern integrated bridges contain safety features that try to prevent similar conditions.

4.2.8 Position sensor

The position sensor is a critical component for actuator control. It provides information for the controller, which uses it to create an action for the control circuit. In the event of a sensor fault, the actuator could be overloaded or damaged by the control unit, which would try to drive to the incorrectly measured position. Depending on the sensor type, common problems such as offset, drift, nonlinearity, gain error, hysteresis and noise [6], [25].

4.3 Additional actuator blocks

Some actuators may be equipped with supplementary sensors that can be used for control purposes and FDD or condition monitoring.

4.3.1 Force sensor

The force sensor is usually designed as a flexible member with a foil strain gauge bridge. The life of the strain gauge is determined by how much stress it is stressed. In general, lower cyclic loading amplitudes lead to longer sensor life. A sensor fault can occur if the maximum permissible load is exceeded. It will cause an overrun from the elastic area to the plastic area and cause irreversible damage to the sensor. If the sensor is stressed to the point of plastic deformation, permanent damage can occur, manifesting an imbalance

of the bridge in the idle position. The detection of these faults can be based on measuring the bridge balance, measuring the change in resistance or monitoring signal losses/failures under cyclic loading caused by cracks in the strain gauge.

4.3.2 Angle sensor

The angle sensor in the form of an incremental rotary encoder (IRC) is prone to defects associated with the degradation of the light source and the sensing element. Faults such as extended sensor pulses, jitter (deviation from true periodicity), encoder stepped pulses, low output pulse levels, extended rising and falling edge duration of pulses or flicker (irregular pulse shape) can occur.

4.3.3 Accelerometers

Accelerometers used to measure vibrations suffer from degradations associated with offset change and gain error [24]. The accelerometer offset does not affect the vibration measurement because it is a DC component. The problem caused by gain error manifests as a change in the amplitude of the measured vibrations. Another problem may be the attachment of the accelerometer to the structure. In the case of loosening, reflected by the change in the stiffness of the accelerometer-object connection, the frequency response and sensitivity change fundamentally.

4.3.4 Temperature sensors

Temperature sensors are prone to degradation, especially related to thermal stress and material ageing. These degradations are most commonly manifested as sensor offset and gain error, and some sensor types may also exhibit hysteresis and linearity problems. For temperature sensors, the response speed is also important, which can deteriorate in poor sensor attachment due to, for example, vibration or thermal expansion of the material.

4.4 Analysis of relative probability and criticality of faults

The fault analysis of the electromechanical actuator is based on the article [6]. The information from the article has been modified and supplemented to meet the needs of an EMA with a brushed DC motor. The outcome of the analysis is shown in the Table 4.1. The Table contains information on the frequency of faults, which is defined as the relative probability of occurrence, and the relative criticality of faults. Parameters range from 1 for low to 10 for high.

Component	Failure	Probability	Criticality
Motor	Rotor - winding short	5	5
	Rotor - open winding	4	4
	Rotor - imbalance	3	6
	Commutator - wear	4	8
	Stator - complete magnet separation	2	10
Connectors and cables	Short circuit	5	10
	Intermittent contact	5	10
	Insulation damage	5	8
	Fault on soldered joints	5	8
Mechanical transmission	Bearings - spalling	5	3
	Bearings - binding/sticking	2	4
	Bearings - corroded	2	5
	Bearings - backlash	7	3
	Gears	2	6
Leading-screw	Spalling	5	3
	Excessive wear (backlash)	7	3
Nut	Spalling	5	3
	Excessive wear (backlash)	7	3
	Binding/sticking	5	3
	Bent/dented/warped	1	5
Body/housing	piston/rod - crack(s)	1	10
	Mountings - crack(s)	1	7
Power supply and control unit	Cables - short/open circuit	5	10
	Intermittent performance	5	8
	Thermal overload - dielectrics breakdown	6	10
	Degradation of capacitors	4	8
	Degradation of transistors	2	8

Table 4.1: Analysis of relative probability and criticality of faults

4.5 Summary

A typical linear electromechanical actuator consists of a motor, gearbox, lead screw, nut, cover, supply cables and additional components such as a control unit, power electronics and sensors. Each of these components is prone to failure in different ways, and the frequency and probability of occurrence vary.

This chapter contains a detailed analysis of the EMA with a brushed DC motor. The analysis describes the individual elements of the actuator and its components. For each part, the faults that may occur in a given element and the mechanisms leading to these faults are described. In addition, the analysis is supplemented with information about the

possibilities of monitoring potential defects and degradations. The analysis ends with a Table summarising the relative probability and criticality of faults. This Table was created based on the available literature and has been modified to meet the needs of EMA with a brush DC motor.

Based on the analysis presented in this chapter and the requirements of a non-intrusive approach, specific faults further investigated in the presented thesis are selected.

Chapter 5

Design of FDD methods

5.1 Defect selection

The current trend in the fault detection and diagnostics of electromechanical actuators is leaning toward decentralised solutions [8], [19], [36]. The high degree of integration and good availability of components suitable for measurement and data processing allows performing diagnostics directly on the actuator. This solution, sometimes called a smart or intelligent actuator, comprises an actuator with a dedicated unit responsible for integrated monitoring, controlling, and evaluating health status [8]. Outputs of the local diagnostics are represented by individual indicators; their values are then passed to superior systems, which evaluate the overall operability. The FDD of EMA presented in this thesis follows idea of distributed dedicated monitoring.

The key principle of proposed fault detection for EMA with brushed DC motor is the non-intrusive approach. The main goal is to design fault detection methods that do not require additional components, EMA modifications, unique installations, sensors or sources of information. A suitable solution that withstands listed requirements lies in the use of motor current measurement. The main advantage of this approach is that it does not require intervention in the actuator. The current can be measured either with current clamps on the supply cables or using the control unit. In addition to the standard protection elements, highly integrated control units are usually equipped with the current senors. In the case of devices driven by PWM, such as brushed DC motors, the control unit may provide measurements of the current flowing through the H-bridge transistors.

The unique features of the brushed DC motor current signal can be utilised for fault FDD. However, the amount of information contained in the signal is limited, and therefore such defects must be selected, the detection of which is unambiguous and unmistakable. The selection of specific faults is based on the analysis of EMA faults described in chapter 4. This analysis provides information about the effects of individual failures and their relative probability and criticality. These criteria were taken into account to select defects:

- **Selected defects are reliably detectable in the motor current:** The mani-

festation of different defects can vary significantly. Some may not be detectable, and others may be hidden in the signal. It is necessary to focus on such faults, which are detectable in the signal in all operating modes of the actuator.

- **They have a high level of probability of occurrence and criticality:** The level of both values can vary for each type of failure. The most worrying defects are those for which none of the parameters is low. By comparing the multiple of both parameters, it is possible to obtain information about the severity of individual faults (see Table 4.1).

- **The manifestation of them is similar for a variety of brushed DC motors:** Brushed DC motors can vary in many parameters such as maximum power, nominal current, torque, maximum speed, number of winding coils, or commutator segments. The effect of selected faults should manifest in the same way regardless of parameter composition.

The specific defects are selected considering the above mentioned criteria and characteristics of current signal.

5.1.1 Signal description

The fault detection methods can be based on evaluating the features of electric current specific for EMA with brushed DC motor. The typical current waveform, influenced by mechanical and electrical properties of the actuator, can be seen in Figure 5.1.

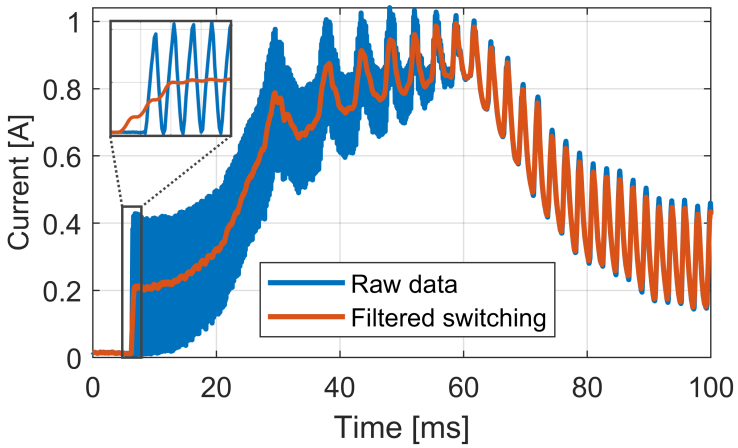

Figure 5.1: Electric current during the controlled run-up of EMA with zoomed detail of switching effect

A PWM control of motor speed causes the high-frequency component in the raw current. The current switching is driven by a PWM signal, defined by the frequency f_P and duty cycle D expressed in percentage. The frequency of PWM (f_P) should be high enough to

have the switching period lower than the time constant of the motor coils. The effect of switching is more noticeable at lower values of D and completely disappear at D =100 %. It can be seen in Figure 5.1 during the motor run-up. The D is about 50 % at the beginning to decrease the inrush current. It increases up to 100 % with the rise of the motor speed, and the effect of switching disappears.

The low-frequency oscillations in the waveform are caused by commutation spikes, which occur when the brush breaks the contact with the commutator sector connected to the energized winding. Figure 5.1 shows the filtered signal where the switching effect was suppressed, while commutation spikes are still visible. Commutation spikes are directly related to motor rotation, and therefore, this information might be used to detect actuator jams. In addition, the electrical imbalance of commutation spikes can be used to monitor windings conditions. Based on these findings, the thesis further elaborates methods for detecting EMA jams and winding shorts of motor.

5.1.2 Jam fault description

The actuator jam is caused by a fatal failure of its components. There are a number of mechanisms that can lead to jams as a result. The most common factors are excessive overload or wear, insufficient lubrication of moving parts, mechanical damage or thermal stress, manufacturing defects or poor maintenance. The analysis in chapter 4 points to several specific faults causing the jam of the actuator, such as loose magnets due to thermal stress, fatal damage of the mechanical transmission due to severe overload, insufficient lubrication of moving parts (screw, nut, bearings or mechanical transmission), permanent deformation of some actuator parts or excessive external load. As a result, the jammed actuator cannot move, which causes further overloading and the possible extent of the damage.

The jam of the actuator results in increased currents. The overcurrent protection might be used as a countermeasure against the jam; however, it is not efficient for all modes of operation. The first problem is the high inrush current that must be considered. The inrush current manifests by a high current spike, which disappears when the winding is magnetised during the motor run-up. This phenomenon usually takes tens of milliseconds, but the peak value may overcome the nominal current multiple times. An example of an inrush current can be seen in Figure 5.2. This example shows that the actuator with the maximum rated load of 2 A may have more than three times higher current spike. The overcurrent protection should be set close to the maximum rated load, but at the same time, its reaction must not be too fast. Otherwise, it would switch off the motor during each uncontrolled run-up.

The second issue is that the magnitude of the current during a jam depends on the specific operating conditions. The actuator can be deliberately controlled at lower power ratings, for example when controlled by a force sensor that limits the maximum available force. Under these conditions, the actuator is operated at low PWM values, which results in a lower motor current. If a jam occurs, the maximum current value may not exceed the rated current of the actuator at all. However, this condition is still severe because

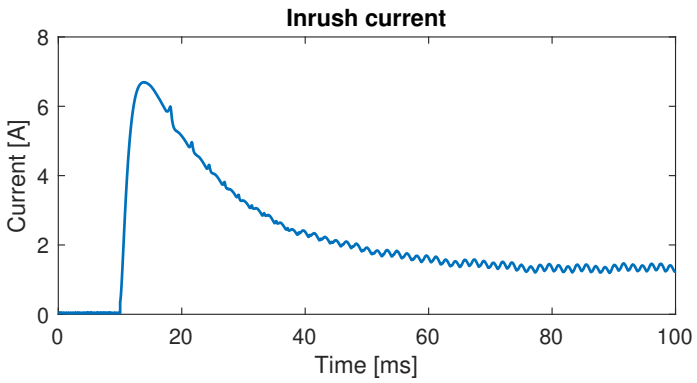

Figure 5.2: Inrush current during the motor run-up

the actuator cannot move under the given conditions. A similar situation can occur if the motor's voltage is intentionally reduced to reduce the overall power. Simple current protection would be unsatisfactory in these cases, and no jamming would be detected.

Actuator jamming is a serious problem that requires considerable attention. In this thesis, a method for jam detection for electromechanical actuators with a brush DC motor is designed and validated.

5.1.3 Winding short fault description

Electrical faults in motors are among the most common faults in electromechanical actuators [6]. The rotor winding shorts arise in the case of insulation failure between coil turns. The most critical are shorts between the individual coils of the rotor [25]. It is usually caused by the degradation of the insulation due to thermal effects, contamination or centrifugal force (the more detailed overview of winding short causes is provided in [1]):

- **Thermal effects** - thermal damage of the most commonly used insulating varnishes manifests in an oxidative chemical reaction. The bonds in the organic parts of the insulation can break at sufficiently high temperatures. Thermally-induced vibrations can cause chemical bonds breakage. The degraded material is more brittle and has lower mechanical strength. Thermal damage is caused by overloading, poor engine design, poor production, insufficient maintenance or pollution. Manifestations of thermal overload depend on the type of insulation and are characterised by peeling, cracks, leakage or discolouration of the insulation.

- **Repeated overvoltage** - high peak voltage applied to the coil can cause a partial discharge in places where the wire is not well insulated (e.g. air gap). Repeated partial discharge can break the insulation in points or reduce its insulation properties. This phenomenon depends on the size of the voltage peaks and manifests itself only at higher values. It is unique in machines operating at low voltage, but it can occur during transients caused by fault conditions.

- **Contamination** - contamination of the windings leads to many problems, including increased thermal damage (due to blocked air ventilation) or chemical damage, where degradation of the insulation materials can occur. Dust, iron dust from other components, fly ash, oil leaking from the bearings, moisture from the atmosphere or other chemicals attacking the insulation materials can be considered as sources of pollution. Another problem is the ingress of particles that have an abrasive effect. Such particles can mechanically damage the winding insulation to the point where it is completely exposed and therefore prone to short circuits. Signs of the contamination may appear as greasy or wet films on the engine and may also be accompanied by dark carbonised marks.

- **Centrifugal force** - the centrifugal force acting on the components of the rotor winding insulation system tends to deform the coil conductors and disrupt the coil insulation. If this system is released, vibrations may occur, which will cause the insulation to abrade. These phenomena occur when the rotor coils are incorrectly attached. Attachment failure can be caused by mechanical stress, poor construction or material defects. Unbalanced rotor, frequent turning and braking or exceeding the maximum speed can have a similar effect. Deformations caused by centrifugal force can manifest as increased engine vibrations.

The defect of shorted winding causes a reduction in torque, which usually does not lead to a complete loss of EMA function. This defect is exhibited by a change in resistivity, inductance, and the back electromotive force's magnitude. The extent of these changes depends on the number of shorted turns and arranging the winding [25]. The effect of winding short can be seen in Figure 5.3. The motor's electrical imbalances, caused by

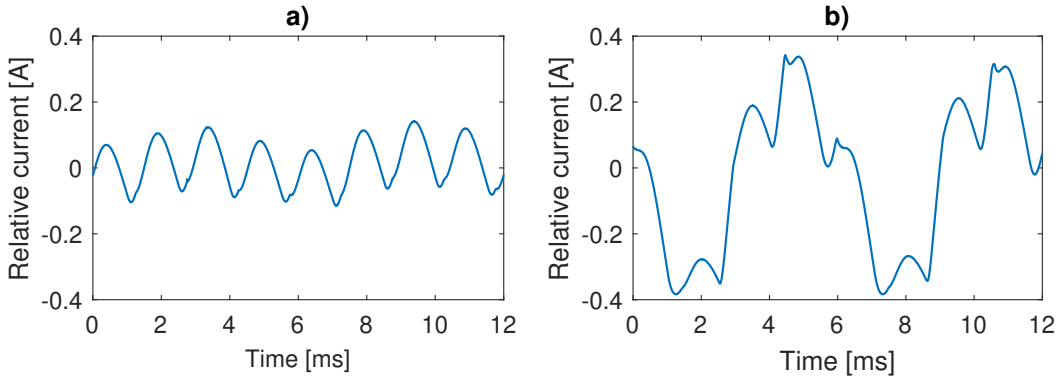

Figure 5.3: Relative current measured during one revolution of the motor with 8 commutator segments: a) electrically balanced winding, b) winding affected by a short

winding short, can result in decreased motor efficiency, weakening magnetic fields, increasing current, overheating, and vibrations.

Due to the severity and high probability of a winding short, a new fault detection method is presented in this thesis. This method is designed dedicatedly for electromechanical actuators with a DC card motor.

5.2 Design of jam detection method

The algorithm of jam detection method is depicted in Figure 5.4. Raw sampled data from

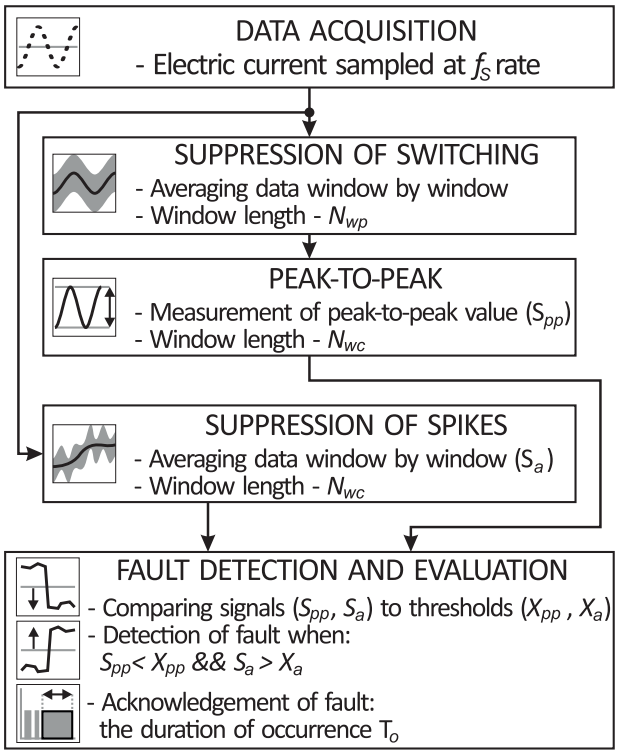

Figure 5.4: Block diagram of the jam detection algorithm

the block "Data acquisition" are first filtered in two branches in order to get rid of specific components contained in the signal (see section 5.1.1). The first block, called "Suppression of switching", suppresses high-frequency components caused by PWM motor control. The output from this block still contains commutation spikes that provide information about the motor's movement. The effect of PWM switching and its suppression can be seen in the zoomed detail of Figure 5.1. The second filtering block, called "Suppression of spikes", aims to eliminate both high-frequency PWM switching components and low-frequency commutator oscillations. The output represents averaged motor current over time and gives the information on whether the motor is under load.

Standard digital filters (FIR/IIR) can be computationally intensive; in this paper, a different approach was chosen. The filtration has been done by averaging data with different windows length without overlap. This approach worse resolution in time but

reduces computational complexity. Since the size of filtering windows is derived from the EMA parameters, the data produced by filters are still suitable for fault detection, despite the degraded time resolution.

The length of the window for suppression of switching is based on the sampling frequency f_S and PWM switching frequency f_P as

$$N_{wp} = a \cdot f_S / f_P \tag{5.1}$$

where N_{wp} is the length of the window, a is the factor that extends averaging over multiple periods, and the f_P is the lowest PWM switching frequency.

The suppression of commutation spikes is based on the EMA's lowest speed of a motion. The length of the window for suppression of commutation spikes is calculated as

$$N_{wc} = f_S \cdot T_{max} \tag{5.2}$$

where N_{wc} is the window's length, f_S is the sampling frequency, and T_{max} is the longest time of commutation spike measured during the slowest possible movement of EMA without load.

The filtered data with the commutation oscillations are used to detect movement, while the filtered data without oscillations are related to load. The proposed algorithm measures a peak-to-peak (pp) value of the signal with commutations for motion detection. This value is calculated using the window with a length equal to N_{wc}. This parameter is also computed without overlap to reduce computational complexity.

The last part of the algorithm is the fault detection and evaluation that process peak-to-peak and averaged signals. The presence of significant values of the peak-to-peak signal represents the rotation of the motor. In contrast, low values mean that the motor is not moving. The X_{pp} threshold is used to distinguish these two states. In the case when the motor is not moving, it can be either jammed or stopped. The averaged current is used to assess these situations by comparison with the X_a threshold. If the average current is above the X_a and at the same time the peak-to-peak signal is below X_{pp}, a fault is detected. The peak-to-peak signal and averaged current values can substantially vary during operation, mainly due to the change in load, movement speed, and operating regimes. Thresholds must be set accordingly to cover all possible states. They can be determined from the measurements on EMA without any load at the lowest possible speed. Values of peak-to-peak signal and averaged current are minimal in this condition compared to all possible states during the nominal operation of EMA. The proposed method uses thresholds that are established as 50% of these minimal measured values to ensure acceptable margins. This selection covers all possible regimes of EMA operation, and therefore it is applicable for fault detection.

When a fault is detected, it is acknowledged by the duration of occurrence. It is assumed that the jammed actuator remains in this state for some time. The acknowledgement procedure prevents incorrect identification of faults that may occur during the slow movement of the actuator. A necessary condition is that evaluation time T_o is always higher than T_{max}.

5.3 Design of winding short detection method

During the operation of the brushed DC motor, the damaged winding is energised twice in one revolution, every time with opposite polarity. Thus, the increased current's electrical imbalance should be noticeable at twice the motor's speed. The motor current signal analysis shows that the commutation peaks' dominant frequency is a multiple of the motor's speed. The relation between the motor speed expressed as motor frequency f_M, fundamental commutation frequency f_C and frequency of winding short fault f_{ws} can be described by the following equations

$$f_C = N_C \cdot f_M \tag{5.3}$$

$$f_{ws} = 2 \cdot f_C / N_C = 2 \cdot f_M \tag{5.4}$$

where N_C is number of commutator segments given by commutator arrangement.

The algorithm for winding short detection is depicted in Figure 5.5; it comprises four parts; data sampling, data selection, spectrum analysis and fault evaluation.

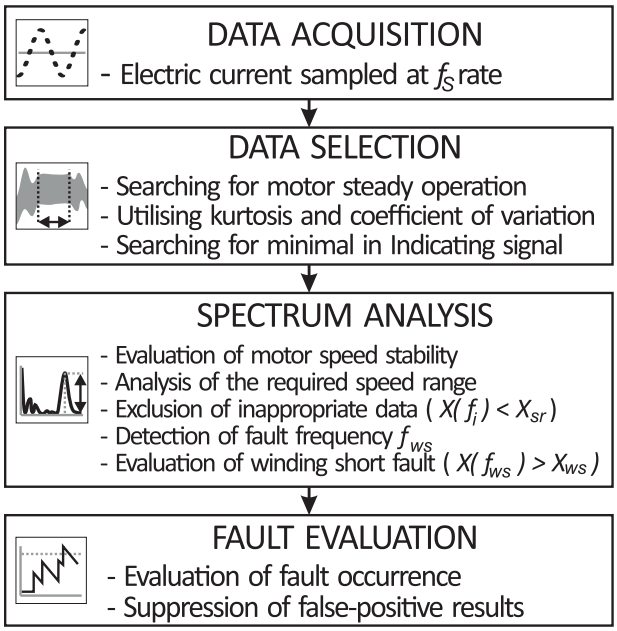

Figure 5.5: Block diagram of the winding short detection algorithm

The sampled data are processed in windows of the length based on the system's parameters, such as the maximal speed of rotation and number of measured rotations. The measured time interval should be short of catching the motor's steady operation but with reasonable resolution in the frequency spectrum. Also, it should be long enough to capture periodicity in the measured signal. Therefore it is preferable to perform the detection at

higher motor speeds. The measured time interval is established for 50% of motors speed as

$$T_d = r \cdot 60/(v_{max} \cdot 0.5) \tag{5.5}$$

where r is a number of revolutions required for analysis and v_{max} is the maximal rotation speed of the tested motor in RPM (Revolutions Per Minute). The resolution in the frequency spectrum is directly related to the measured time interval, and it is described as

$$f_\Delta = f_S/N_W = f_S/(f_S \cdot T_d) = 1/T_d \tag{5.6}$$

where f_S is the sampling frequency and N_W is the length of the window. Ten per cent or lower values of the lowest frequency of interest should be sufficient resolution for spectrum analysis.

The electromechanical actuators can be controlled to a specific position, to required motion profiles or other desired parameters based on the particular use case. Rapid control actions of the controller cause dynamic changes in the EMA's speed and direction of movement that are also reflected in the measured current. The proposed method brings a novel approach to dealing with the dynamic changes of EMA behaviour during control; the fault detection is provided in short time segments where the signal is near a steady state. The kurtosis is used to assess steady state; outliers primarily determine its value [20]. It reaches highs when the signal is not regular, and conversely, lows indicate a steady state. The motor current signal can also vary with the speed and load; the coefficient of variation is used to compensate for these fluctuations. Multiplying these parameters produces an indicating signal that is calculated over the T_d period as

$$I_s = k \cdot \widehat{c_v} = \frac{\frac{1}{n}\sum_{i=1}^{n}(x_i - \overline{x})^4}{\left(\frac{1}{n}\sum_{i=1}^{n}(x_i - \overline{x})^2\right)^2} \cdot \frac{s}{\overline{x}} \tag{5.7}$$

where k is kurtosis, $\widehat{c_v}$ is coefficient of variation, n is number of samples, $\overline{x}$ is mean and s is standard deviation. The minimum in every ten samples of the indicating signal is used to select data that are suitable for subsequent analysis.

The detection of a winding short fault is based on the Motor Current Signature Analysis (MCSA) [40], [41] using amplitude spectrum. Spectrum analysis is performed only on the block of data that the data selection procedure provided. The length of the window for analysis given by the T_d is therefore always the same. The main goal of this analysis is to identify f_C and then search winding short fault represented by f_{ws}. The spectrum is gradually analysed in different ranges depending on the maximum engine speed. The border frequencies of desired range can be expressed by the f_C as

$$f_C = D_M \cdot N_C \cdot v_{max}/(60 \cdot 100) \tag{5.8}$$

where D_M is the desired percentage of maximum motor speed.

The first step of the algorithm is to find a significant peak (f_i). The spectrum is analysed at a narrower frequency range corresponding to 50 to 100% of maximum motor speed at first. Only the fundamental frequency of f_C or its second harmonics f_{2C} should be present within this range. When no significant frequencies are found, the range is extended to 25 to 125%, and the process is repeated. This wider range is beneficial in cases when the motor is rotating faster than maximal RPM given by the manufacturer (actual f_C is higher than maximal expected f_C refer to 5.8) or slower than 50% when the peak of second harmonic is insignificant. However, the analysis in the narrower frequency range must always be performed first to prevent confusion of higher harmonics of f_C with fundamental in the broader range. The required range of the spectrum is always searched in descending order until a peak is found. If no significant peaks are found, the tested block of data is discarded. Otherwise, the amplitude of the founded peak is compared to the mean value in this range. The low ratio between them indicates the changing motor speed (smeared peak), and the data block is also excluded from the analysis. The peak with a high ratio is further investigated. The threshold for this step (X_{sr}) can be determined based on measurements conducted during nominal operation at the 25% of speed and without load, because the amplitude of f_C reaches the lowest values acceptable for analysis. It might be established as a multiple of mean value that is still lower than the amplitude of f_C at this speed.

The next step is to verify whether the frequency of the investigated peak (f_i) is the fundamental commutation frequency (f_C). The amplitudes at f_i and $f_i/2$ are compared. If the amplitude of $f_i/2$ is higher than amplitude at f_i, it means that $f_i/2$ is fundamental commutation frequency (f_C). Otherwise, f_i is the fundamental commutation frequency. Founded f_C is used for fault detection. The detection is based on searching for the significant amplitude at twice f_M (refer to (5.4)). The height of the peak f_{ws} reflects the extent of the fault, which allows degradation monitoring. The X_{ws} threshold defining the fault can be established by comparing amplitudes of f_{ws} and f_c.

The fault evaluation is used to suppress unwanted false-positive results by the failure/pass counting. Identified failures increment error value faster than passes that decrement error value. When the error value overcome the preset threshold, the motor's fault is indicated.

5.4 Summary

Diagnostics based on measuring the current flowing through the actuator motor is an ideal means of meeting the requirements of the non-intrusive approach. The thesis deals with the faults of the electromechanical actuator with a brushed DC motor. Detection methods were designed for actuator jam and winding short faults, which were selected based on the proposed analysis and unique features of the current signal.

Several mechanisms can lead to the jam of the actuator. The most common factors are excessive overload or wear, insufficient lubrication of moving parts, mechanical damage or thermal stress, manufacturing defects or poor maintenance. Detection of this fault is based

on monitoring the commutator spikes in the current signal. These spikes are obtained from the signal by filtering data windows with a predefined length. Windows without overlapping are used in data processing, which reduces computational complexity. The presence of spikes in the signal indicates motor rotation. This indicator is compared with the average current flowing through the motor, which reflects the activity of the actuator. The absence of commutator spikes combined with large average currents indicates an actuator jam. A jam alert is reported if such a condition is detected and persists. Detection thresholds are derived from the basic electromechanical properties of the actuator.

The detection of a winding short circuit is based on the assumption that damage to the winding cause an electrical imbalance. It is manifested by an increase in the current of the commutation spike, twice per revolution. The fault can thus be detected as a signal with frequency at twice the motor speed. However, the dynamic behaviour of the actuator does not allow to perform such an analysis directly. First, selecting the time blocks in which the motor speed is constant is necessary. For this purpose, a unique procedure was designed, which uses the kurtosis and the coefficient of variance to process the signal and select blocks with no abrupt changes. This selection produces blocks of data that are further processed in spectral analysis. The first step is to identify commutation frequency, which directly corresponds to the motor speed. The signal with the frequency corresponding to fault is then searched in the spectrum based on commutation frequency. If a fault is identified, multiple acknowledgements are awaited. This verification principle increases detection validity and reduces the chances of false identifications. In addition, the method is equipped with mechanisms that evaluate the validity of the processed data and eliminate inappropriate samples. These mechanisms contribute to decreasing computational complexity and improving overall reliability.

Chapter 6

Testing system

The proposed methods must first be tested and verified by experiments. For this purpose, an automated test system was designed and constructed.

6.1 Block diagram

The block diagram describing the connections of the individual parts of the system is shown in Figure 6.1. The system is controlled from a computer connected to two NI cDAQ - 9174 via USBs. Both units are equipped with three plug-in modules and are controlled by a program from LabView. The upper NI cDAQ - 9174 chassis serves as the primary unit for controlling the rig and the elementary data collection. It includes the NI 9401 module, which provides two-way digital communication with eight digital I/O connectors. It is used to control the actuator motor's direction of rotation and generate a PWM signal. NI 9222 and NI 9215 modules are used to measure a voltage with a resolution of 16 bits. The NI 9222 allows synchronous measurements of up to 500 kS per channel, and it is used for a high-speed recording of the current and voltage waveforms. The motor current is measured on the output pin of the control unit, whose voltage corresponds to the current flowing through the bridge. The motor voltage is measured on the voltage divider connected directly to the power output of the control unit. The NI 9215 allows synchronous measurements up to 100 kS per channel, and It is used to measure slowly changing signals such as position and force.

The secondary NI cDAQ - 9174 chassis include modules for additional measurements. The NI 9234 measures signals from two integrated electronic accelerometers (A1, A2) with the sampling rate up to 51.2 kHz. Additionally, each module channel is equipped with anti-aliasing filters that automatically adjust to your sample rate. The NI 9217 is a resistance temperature detector (RTD) module that provides per channel current excitation. Up to four sensors can be connected to the module with the sampling rate up to 400 Hz between all channels. The NI 9401 in the secondary chassis is used to process TTL signals from Incremental Rotary enCoder (IRC). All additional sensors can be placed anywhere on the test system as needed. The basic configuration for one actuator includes measurement of

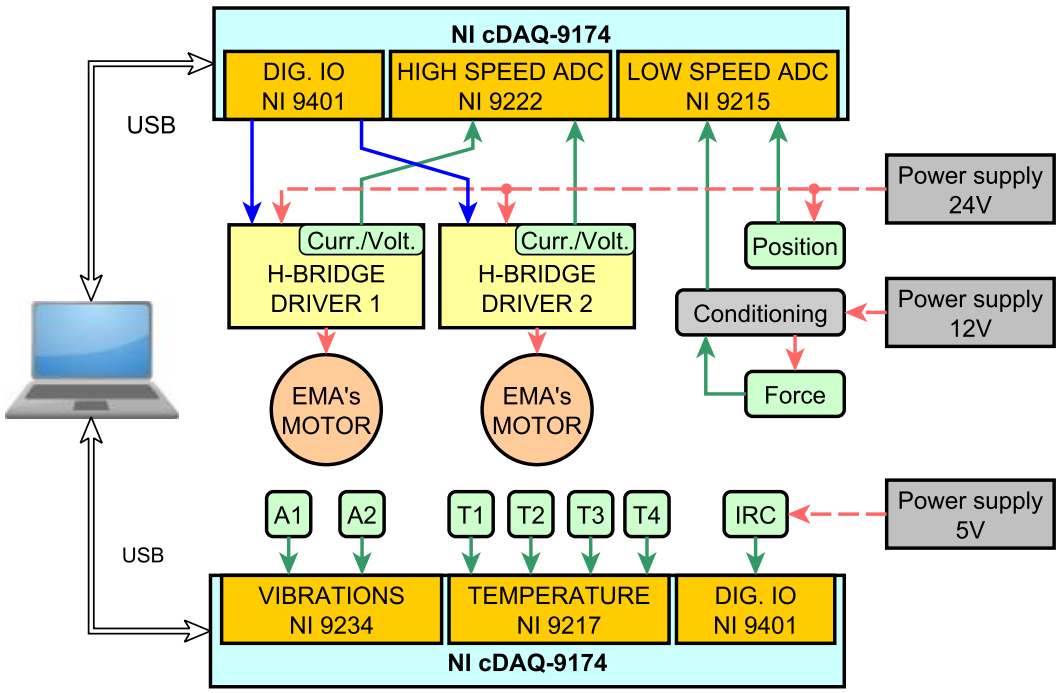

Figure 6.1: Block diagram of the testing system

ambient temperature, the temperature of motor cover, gearbox and casing of rod, vibrations of motor and gearbox and revolutions of the motor.

The diagram also includes power blocks with 5, 12 and 24 V power supplies.

6.1.1 Sensors

The system is equipped with four primary sensors that monitor the position of EMA, the load applied to EMA, the electric current flowing through the actuator's motor, and the voltage at the motor's input.

The position sensor is mainly used as feedback of the control loop of the controller. The test system uses Honeywell's SPS-L225-HALS sensor. This magnetic sensor with analogue output measures non-contact position using a permanent magnet attached to the moving part of the structure. The sensor range is 225 mm, with a resolution of 0.05 mm.

A bidirectional force sensor is installed between the actuator mount and the moving part of the structure. The sensor is used both to measure the actuator force applying on the structure's moving part and as feedback for the control loop. The system uses sensor 151 S-Beam Load Cells from manufacturer Honeywell with a range of ±500 N.

The motor's electric current is usually measured at the motor power driver's output, which contains a current to voltage converter. The output voltage corresponds to the

Table 6.1: Parameters of sensors

Measurement	**Range**	**Sample rate**
Force	±500 N	1 kHz
Position	225 mm	1 kHz
Motor current	15 A	200 kHz
Motor voltage	±32 V	200 kHz
Temperature	-30/200 °C	100 Hz
Vibrations	peak 60 g, 0.3-6000 Hz	51.2 kHz
Motor rotation	200 PPR	up to 20 kHz

current flowing through the H-bridge. The alternative option is the use of the active current clamp with voltage output. The system is equipped with the Fluke i30s, the AC/DC current clamp based on Hall Effect technology. The main advantage of measurement with this sensor is the high-frequency range from DC up to 100 kHz, suitable for transient effects measurements.

The voltage on the motor of the actuator is measured using the voltage divider, which is connected between the output of the H-bridge and the motor's input. The divider was designed that it is possible to measure up to ±32 V. In this range, the output of the divider stays under the 10 V, which is the limit for the differential analogue input of IN 9222.

The system is equipped with additional sensors such as temperature sensors, vibration sensors, and incremental rotary encoder. These sensors can be placed in the system as needed.

There are four miniature Pt100 4-wire RTD (NB-PTCO-155) sensors that can be attached to any part of the system. The range of temperature sensors is -30 to 200 °C. For the vibration measurement, there are two Bruel&Kjaer 4507-B-004 accelerometers that have vibrations range 0.3 to 6000 Hz up to peak 70 g. Additionally, these sensors are also TEDS (Transducer Electronic Data Sheet) compatible. For the measurement of the motor revolution, there is an Incremental Rotary enCoder. The used HEDR-5421-EP111 is the two-channel optical incremental housed encoder that has a resolution of 200 PPR (Pulses Per Revolution) per channel.

The operating ranges and sample rates of all sensors are summarised in Table 6.1 and pictures are in Figure 6.2.

6.1.1.1 Conditioning circuit

The force sensor uses a conditioning circuit responsible for generating stabilised voltage and amplifying the output signal level.

The conditioning block circuit is depicted in Figure 6.3. The circuit comprises a 12 V power supply that powers two low-dropout (LDO) linear voltage regulators and voltage

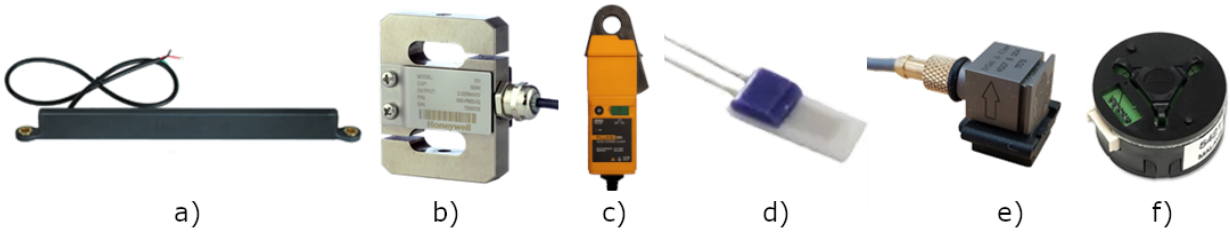

Figure 6.2: Sensors used in testing system: a) position, b) force, c) current clamp, d) temperature, e) vibrations, f) IRC

follower. The linear voltage regulators are responsible for providing stabilised voltage. The stability of the voltage is essential, especially for the force sensor. The force sensor comprises a strain gauge with the output rated at 2 mV/V of full scale. Consequently, with the 10 V input, the sensor's output is 20 mV under full load. This voltage value is too low and can be easily affected by noise. Therefore, the signal must be amplified appropriately and cleared of noise. The output of the strain gauge is amplified by the rail-to-rail precision instrumentation amplifier. This type of amplifier has a high common-mode rejection ratio (CMRR) of about 115 dB, which is indispensable for common-mode noise reduction. The amplifier is powered by the 7 V output from the second linear voltage regulator. The output signal from the amplifier is then filtered by the first-order RC low pass filter. Parameters of the filter can be changed by the replacement of the R or C component as needed. The basic configuration of the filter has a cut off frequency of about 500 Hz. The output of the filter is connected to the voltage follower to prevent excessive loading of the filter. The circuit is placed in the metal box, and all cables of the entire system are shielded adequately in order to suppress noise as much as possible. Photo and complete schematic of the circuit can be found in appendix B.1.

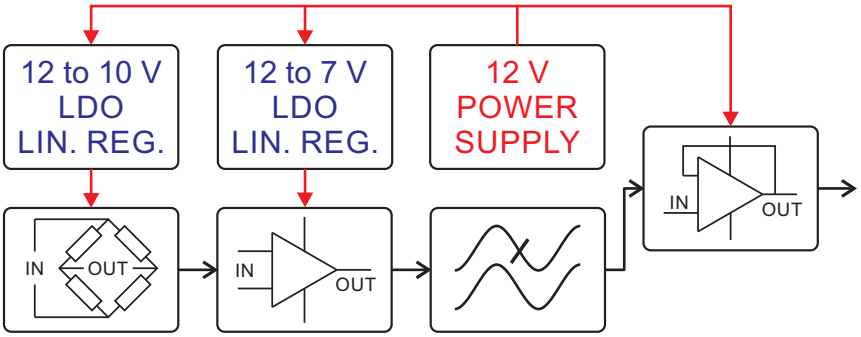

Figure 6.3: Conditioning block circuit

Table 6.2: Parameters of tested EMAs

Parameter	DSZY1	TA 2	Unit
Motor voltage	24	24	V
Maximum load	150	120	N
Maximum speed at 24 V	40 to 45	33 to 44	mm/s
Motor speed at 24 V	6000	4000	RPM
Rod stroke	200	150	mm
Gear ratio	5:1	5:1	-
Typical current	2	1.2	A

6.1.2 Motor power driver

One or two EMAs are connected to their power control driver in the form of a fully integrated H-bridge. The driver uses as input PWM signal defining the power applied to the motor and signals that determine the direction of engine rotation and braking. The unit operates in the 4 – 28 V range and can provide an output current up to 15 A at a maximum PWM speed of 20 kHz. The power transistors have a very low on-state resistance of 70 mΩ. The unit is also equipped with protection elements such as overvoltage, short-circuit protection, thermal fuse, current and power protection or inductive voltage diodes.

6.1.3 Actuators

Two types of actuators with similar characteristics have been used during experiments The TA 2 actuators manufactured by Timotion and the DSZY1 manufactured by the Drive-Systems Europe Ltd. Each actuator consists of a DC motor with the commutator and permanent magnets, speed reducer gearbox and actuator housing with a rod that uses screw and nut to transform rotary to linear motion. The parameters of tested actuators are in Table 6.2.

6.2 Mechanical construction

The mechanical construction of the testing system, which is depicted in Figure 6.4, consists of a frame, a linear guide and mounting parts of individual components such as actuators and sensors. The structure is designed so that it can be changed depending on the requirements of the tested objects.

The frame is composed of lightweight aluminium sections, which have in cross-section of 40×40 mm. The construction itself has the shape of a cuboid with dimensions of 680×488×560 mm, and it is crossed by a bulkhead used for mounting the linear guide and mechanical connector of an EMA. The linear guide is intended to ensure the linear

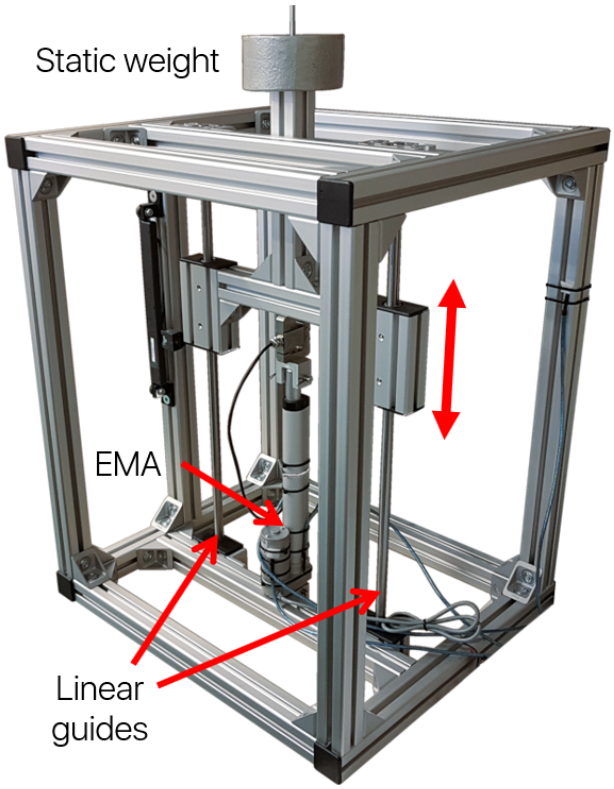

Figure 6.4: The mechanical construction of the testing system with the DSZY1 actuator

movement of the actuator. It consists of two cylindrical rods, on which the trolley fixed by an aluminium profile moves. The guide length is 600 mm, and the carriage height is 120 mm, which allows a range of movement of almost 480 mm. The detail of the linear guide with a trolley is depicted in Figure 6.5.

The construction allows two types of stressing of EMAs. The first is with the static weight. In this case, the weight is placed on the top of the movable part of the construction. The load is scalable thanks to the different weights of the metal blocks that can be placed on each other. The static weight represents load in a constant direction. The actuator is stressed when pushing the load and relieved when pulling. The holder for the static weight can be seen as an upright rod attached to the carriage at the top of Figure 6.5.

The second type is the controlled load achieved by the secondary actuator. In this case, a secondary actuator is controlled based on the pressure sensor and creates artificial weight for a tested actuator. This arrangement allows stressing the tested actuator in both directions. The force is also scalable based on secondary actuator performance.

The proper operation of the artificial load has been achieved thanks to a flexible element that is placed between the load actuator and the construction. This element is necessary for suppressing shocks that are caused by the rigidness of the construction and actuators. A bidirectional damping spring has been designed for this purpose. The spring is made of

Figure 6.5: The detail of linear guide

polylactic acid (PLA) plastic and printed on the Prusa 3D printer. The damping spring is depicted in Figure 6.6.

Figure 6.6: The detail of the damping spring made of PLA

6.3 Software

The test device is controlled by a program designed in LabView. The program allows working with actuators in three different modes of operation: basic motion, position control and load control. Depending on the mode of operation, it is possible to set the duration of operation and PWM frequency. The basic motion mode allows selecting the actuator, the direction of movement and the duty cycle of the PWM. In the position control mode, which uses information from the position sensor, it is possible to select the actuator and use the function generator to define the motion profile, period length, and motion range limits. There are four profiles to choose from: sine, rectangular, triangular and saw. The movement is controlled by a software PID controller. In load control mode, the position control mode is extended by another adjustable PID controller that simulates a load using the force sensor information using a second actuator. In this way, it is possible to execute a predefined motion profile by one EMA, which second EMA will load. The program allows data acquisition from all inputs from the NI 9222, NI 9215, NI 9234, NI 9217 and NI 9401 modules, which it stores in a predefined location with a timestamp indicating the date and time of recording.

6.3.1 Data processing

The data acquired by the testing system must be post-processed for later analysis. Some data can be obtained in the correct format using the settings directly in Labview. These measurements include the voltage, temperatures and vibrations. The voltages are directly measured with the synchronous, high sample rate, 16-bit ADCs (analogue to digital converters). Temperatures are averaged during measurement for maximum possible noise suppression. Averaging reduces the sampling rate to the order of sample units per second, but this rate is also sufficient due to the slow development of temperatures. The vibration measurement includes the calibration coefficients of the accelerometers used, and the output values are directly in predefined units such as g or m/s^2.

The rest of the measured values must be recalculated or further processed to obtain the desired quantities. These measurements include the current, voltage across the divider, position, force, and motor speed. According to specific constants, the electric current and voltage are later recalculated from direct voltage measurements. The position and force are measured using the low sampling rate voltage measurement. Acquired values are recalculated to desired quantities based on the conversion characteristics of the sensors used.

Measuring rotation speed with IRC requires an entirely different approach. The NI hardware and Labview software provide direct angular velocity measurement, but the testing system modules are not equipped with this feature. Based on available equipment, the approach that utilises the measurement of signal pulses duration was chosen.

The typical signal from the IRC is shown in Figure 6.7. It comprises two channels (A and B) that provide TTL (Transistor-Transistor-Logic) pulses during the motor rotation. The signals of channels are shifted by 90° to determine the direction of motor rotation. The

number of pulses of one revolution depends on the sensor used. IRC sensor with 200 PPR per channel was used during experiments. The upper part of Figure 6.7 also shows the measurement of the time period. The duration of one pulse is established as the number of internal timebase clock oscillations (see bottom of Figure 6.7.), and it directly depends on the rotation speed. The equipment utilised in the testing system has only one counter that can be used for time measurements. The counter is used for channel A only. Channel B is ignored, and therefore it is impossible to distinguish the direction of rotation directly.

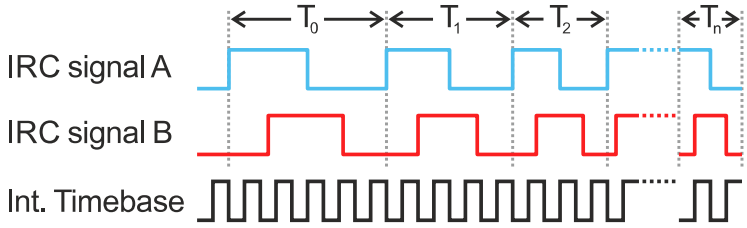

Figure 6.7: Signal from IRC sensor

One of the testing system requirements was to measure the motor speed with the highest possible accuracy considering the available components. Motor speed can be expressed in the frequency of rotation. The precision of frequency measurement depends on the internal timebase frequency and the speed of rotation. The module's internal timebase frequency is 80 MHz, and the highest speed of motor rotation is 6000 RPM. The worst resolution in frequency can be determinate at the highest speed of motor rotation. First, the number of counter increments must be calculated as follows:

$$N_T = T_M F_C = \frac{F_C}{\frac{\omega_R}{60} C_P} = \frac{80 \cdot 10^6}{\frac{6000}{60} \cdot 200} = 4000 \tag{6.1}$$

where N_T is the number of counter increment, T_M is the minimal time period of IRC pulse at given motor speed, F_C is frequency of time base, ω_R is the maximum motor speed in RPM and C_P is the IRC resolution in PPR. Assuming that the resolution step is given by the increment of the counter by one ($N_T 1 = 4001$), the resolution in frequency at a maximum speed of rotation for one pulse is:

$$\Delta F_R = F_T - F_{\tau 1} = \frac{F_C}{N_T} - \frac{F_C}{N_{\tau 1}} = \frac{80 \cdot 10^6}{4000} - \frac{80 \cdot 10^6}{4001} \approx 20000 - 19995 = 5Hz \tag{6.2}$$

This resolution applies to a 1.8° rotation of the motor shaft. It is significantly improved when considering one whole revolution of the motor. In this case, the resolution in frequency will be no worse than $\Delta F_R \approx 0.025Hz$.

The output of the measurements is the series of timestamps that corresponds to the speed of rotation. For each one rotation of the motor shaft, 200 samples are obtained. These data are non-uniformly sampled in time. The sampling is triggered by the motor shaft's angular motion, and therefore measured data are in the angular position domain.

This feature can be used in data analysis because rotary equipment's mechanical and electrical fault signatures are synchronised with the motor's angular position [17]. Since the measured data already contains time information, it is possible to create a time vector of measurement. The sequential addition of measured timestamps creates this vector. It can be used to display the motor frequency's evolution over time and to resample the signal to a time domain with a fixed-rate where it can be subjected to other types of analysis.

This approach's main advantages are single-channel measurement, high resolution in frequency, and the possibility of analysis in both time and angular domain. The disadvantage is that the information about the direction of rotation is missing. For this reason, the internal recording of the direction of the motor rotation has been added. The direction readings are taken from the software controller that drives the movement of the actuator. This indirect method introduces an error in the measurement when the controller requires an immediate change of direction, but the motor has not changed the original direction. This behaviour is caused by the inertia of the actuator that cannot change movement immediately. However, the controller's dynamics, especially the integral component, suppress this error significantly. Furthermore, the gear ratio and insignificant moment of inertia of the rotor compared to the entire actuator's stiffness cause the motor reacts responsively.

The information about the direction complements the angular based measurement of motor speed. It is used for the relative determination of the actuator's rod position. Each motor speed data sample expresses the time it takes to rotate the motor shaft about 1.8 degrees. The actuator's rod relative position can be determined based on the direction of rotation and the rotation to translation ratio.

6.3.2 Data evaluation

Readings from IRC in form angular sampled periods are recalculated to several entities such as instantaneous motor frequency, motor frequency averaged over one revolution, motor speed (in RPM), relative shaft angle and relative position (actuator displacement). Most complex data processing is devoted to calculating the relative position; therefore, this quantity is used for data evaluation. The artefacts caused by the indirect recordings of the direction rotation are shown in Figure 6.8.

This indirect method causes a sharp transition, which introduces an error in relative position. This error is caused by the different timing between the control unit's command and the actual change of direction. The generated time difference is about 15 ms, and the introduced error is about 1 mm. Figure 6.8 shows the worst-case scenario that can occur. This case was stimulated by the sudden change in direction, which was forced at the actuator's full speed. In regular use, such a drastic change does not occur. The integral component of the controller makes a smoother transition that suppresses this artefact.

Figure 6.9 is attached for comparison. The relative position is compared to the data obtained from the absolute position sensor. The data from the absolute position sensor are considered as the reference. Since the relative position always starts at zero, the waveform was shifted 5 mm under the reference data. In this case, the actuator was derived by the position controller. The triangle path was chosen because it contains sudden changes

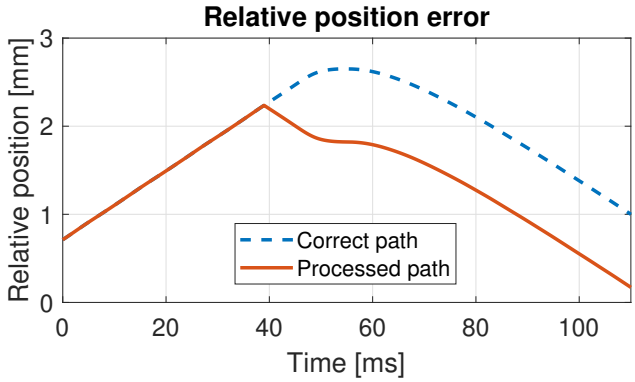

Figure 6.8: The zoomed detail of artefact caused by the indirect recordings of the relative direction

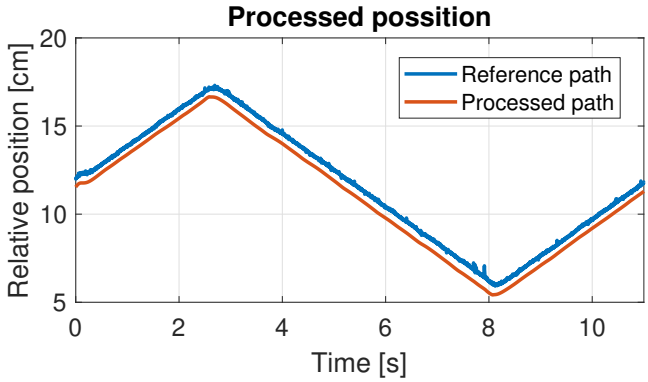

Figure 6.9: The comparison of relative position with reference. The processed waveform was shifted 5 mm under the reference data

in direction. It can be seen that even though the waveform from the IRC contains the transition artefacts, the recorded path profile corresponds to the reference. Measurements have shown that the processed data from IRC can be used to diagnose and analyse EMA.

The main advantage of the relative position obtained from the IRC is that it is not affected by the noise compared to the absolute position sensor. The data from the absolute position sensor are sampled at 1 kHz and averaged by a window of 20 samples in order to get rid of 50 Hz noise. Despite considerable signal smoothing, it is possible to encounter sudden deviations (see Figure 6.9 - Reference path, about 8 s). In contrast, a position from IRC does not contain any unwanted noise peaks. The smooth character of this signal can be beneficial in the case of control, especially for the derivative action.

6.4 Summary

This chapter introduces an automated system for testing electromechanical actuators. The testing system was designed for the development of fault detection and diagnostics methods. The system allows testing various types of linear actuators, measuring parameters during their operation, introducing artificial faults, analysing fault modes, and designing and testing methods for fault detection and diagnosis.

The mechanical construction of the system consists of an aluminium frame, a linear guide and mounting parts of individual components such as actuators and sensors. The structure is designed so that it can be changed depending on the requirements of the tested objects.

The tested actuators are driven by power control units in the form of H-bridges using PWM pulses generated according to the requirements of the control software in the LabView environment.

The system offers automated controlling of the movement of two actuators along predefined paths. The position, force applied to the actuator, the current flowing through the actuator motor, and the voltage at the motor's input are recorded during the tests. Also, secondary parameters such as vibration, temperature, and motor revolutions can be added to the measurement. Data from the IRC sensor that provides a measurement of motor revolution can be used as additional information about relative position.

The actuators can be stressed with the static load, or it is possible to use the second actuator as an artificial load. This configuration makes it possible to run the stress tests under conditions that the actuator would be subjected to regular operation.

Chapter 7

Results of methods testing

7.1 Testing of methods

Both proposed methods were tested over a set of experiments during which various operating conditions were applied. Table 7.1 shows a collection of all operating conditions and their ranges. For each method tested, different combinations were selected to cover all possible operating situations. It is worth mentioning that the measured current is processed in absolute value, and therefore the direction of movement is not apparent from the collected data.

Table 7.1: Various operating conditions of EMA

Variable conditions	**Used in case of**	**Type or range**
Duty cycle	Jam	$20\% \leq D \leq 100\%$
Speed of movement	Both methods	$0\% \leq v \leq 100\%$
Load	Both methods	$20\% \leq F \leq 120\%$
Motion profile	Winding short	Sinusoidal Rectangular Triangular
Injected fault	Winding short	Short within one coil Short between different coils
Mechanical barrier	Jam	Hard barrier Resilient barrier

7.1.1 Testing of jam method

The algorithm for jam detection was verified by a series of experiments. Testing was performed for different working conditions, including the various duty cycles, movement speeds, and loads. Conditions during experiments were determined as follows: $f_S = 200\ kHz$, $f_P = 16\ kHz$, $a = 3$, $N_{wp} = 38$ refer to (5.1) and the longest time of commutation spike was measured as $T_{max} = 67.6\ ms$, therefore $N_{wc} = 13520$ refer to (5.2). This period corresponds to the rod's movement at a rate of $v_{min} = 0.8\ mm/s$, which is about 1.7% of maximum speed. The fault detection thresholds are determined from the measurements concluded on EMA without any load at the lowest speed. Values of commutation spikes span and averaged current are minimal in this measurement compared to all possible states during the nominal operation of EMA. Therefore, thresholds are established as 50% of these values to ensure acceptable margins. The resulting thresholds came out as $X_{pp} = 50\ mA$ and $X_a = 65\ mA$.

The jam fault was simulated using a solid mechanical barrier in the path of the actuator rod. The rod impact into the barrier was either direct (hard stop) or gradual using a resilient insert (soft stop). The example of current change measured during the jam fault is depicted in Figure 7.1. The Figure illustrates the course of averaged and peak-to-peak signals that the algorithm uses for fault detection.

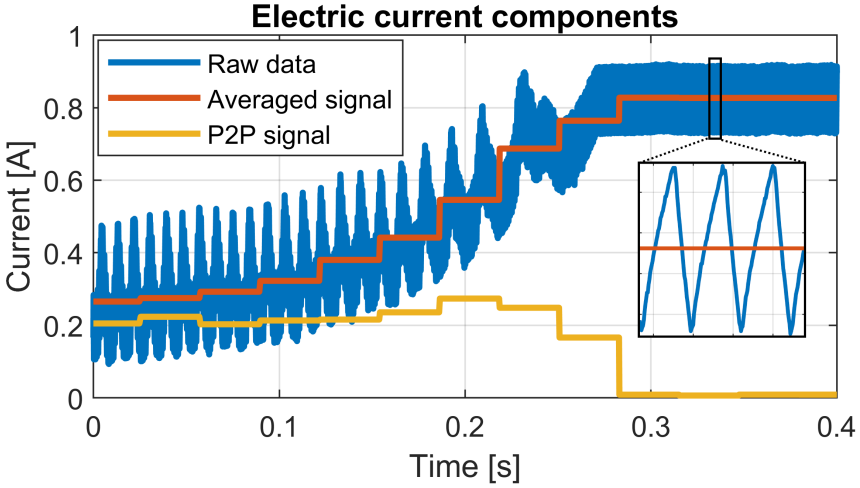

Figure 7.1: The example of calculated components of electric current during the jam of EMA

Two outcomes from method testing are shown in Figure 7.2. The experiment in Figure 7.2 a) was performed with the duty cycle $D = 100\%$ and the evaluation time set to $T_o = 0.1\ s$. The nominal operation can be seen at the beginning of the experiment. After about 500 ms the load is so high then the motor cannot move anymore, and the algorithm detects the fault which is highlighted in the frame called "Fault detection" (values 1 or 0). The detected state is evaluated after the set time has elapsed as a jam fault. This experiment shows the case of a hard stop at the full speed of the actuator. The raw data

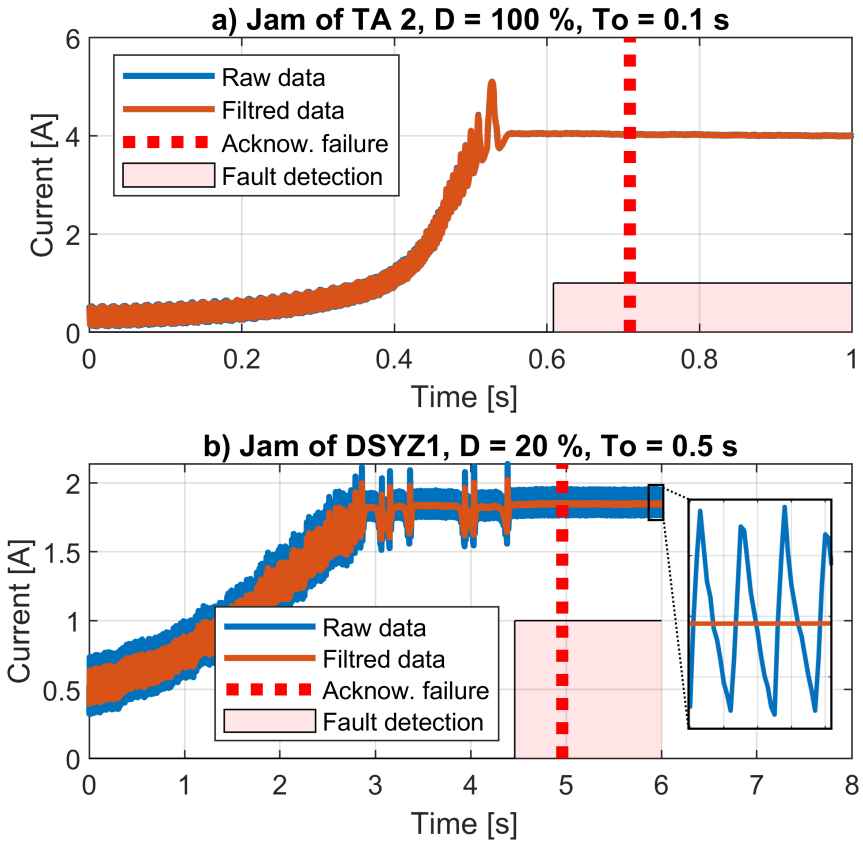

Figure 7.2: Jam fault detection: a) hard stop, b) soft stop

are fully overlapped by filtered data in this case, as explained in section 5.1.1. Figure 7.2 b) shows a situation where the actuator was driven slowly ($D = 20\%$) to a soft stop. Oscillations between 3 s to 4.5 s seconds in the filtered signal demonstrate the deformation of resilient material before the jam.

It can be seen from Figure 7.2 a) and b) that by setting a longer time to acknowledge the fault, false positive detection can be prevented.

Figure 7.2 b) also demonstrates that simple overcurrent current protection would be not sufficient. When EMA is driven using low duty cycles, the averaged current is within the nominal range even when the actuator is jammed.

7.1.2 Testing of winding short method

The winding short detection method was tested during the DSZY1 actuators' faulty and nominal operation. During tests, the actuator was autonomously driven by a controller that moved the rod along predefined trajectories. The function generator produced the position set-point, which formed sinusoidal, triangular and rectangular motion profiles. The EMAs were exposed to loads 20%, 53%, 100%, and 120% of the nominal load for each

Table 7.2: Resistivity and inductance change measured on the commutator segments of the EMA motor

Commutation segments	No defect		Fault 1		Fault 2	
	1 kHz	10 kHz	1 kHz	10 kHz	1 kHz	10 kHz
1, 5	2.7 Ω 1.8 mH	13 Ω 1.7 mH	2.5 Ω 1.64 mH	12 Ω 1.54 mH	3.7 Ω 1.15 mH	10.4 Ω 0.95 mH
2, 6	2.7 Ω 1.77 mH	13.1 Ω 1.67 mH	3.2 Ω 1.07 mH	9.7 Ω 0.94 mH	3.8 Ω 1.09 mH	10.2 Ω 0.89 mH
3, 7	2.7 Ω 1.78 mH	13.1 Ω 1.68 mH	3.3 Ω 1.08 mH	9.9 Ω 0.95 mH	2.7 Ω 1.6 mH	12 Ω 1.5 mH
4, 8	2.7 Ω 1.8 mH	13.4 Ω 1.7 mH	2.5 Ω 1.64 mH	12.1 Ω 1.54 mH	2.7 Ω 1.65 mH	12.3 Ω 1.55 mH

motion profile during experiments. Two faults were injected by artificially shortening the two nearest turns of the rotor coil. In the case of Fault 1, two turns of the same coil were shorted, and in the case of Fault 2, two turns of different coils were shorted. The artificial faults are shown in Figure 7.3.

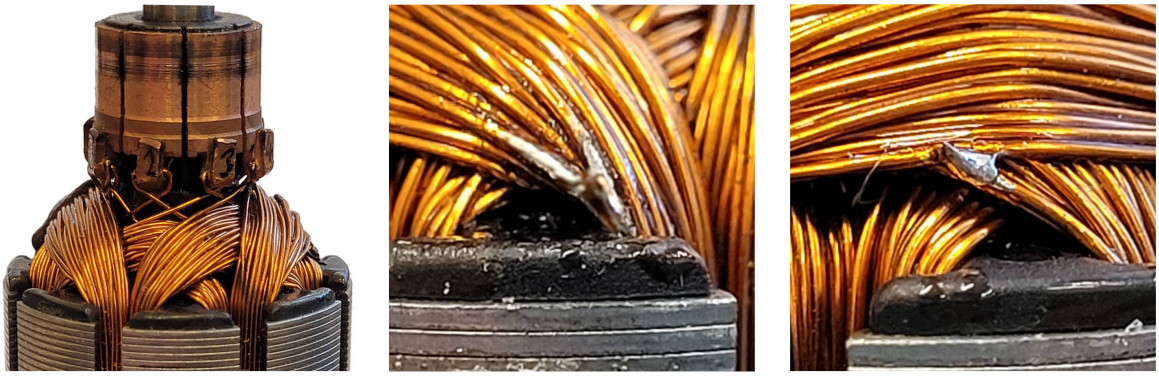

Figure 7.3: Rotor winding - a) intact winding, b) detail of Fault 1, c) detail of Fault 2

The effect of electrical imbalances of motor winding (measured with the precision RLC meter LCR-6020 at 1k Hz and 10 kHz) can be seen in Table 7.2, where the most significant changes are highlighted. Each parameter was measured between two commutator segments.

Conditions during the experiments were determined as follows: $v_{max} = 6000\ RPM$, $r = 10$ thus $T_d = 0.2s$ refer to (5.5), $f_S = 200\ kHz$ and $f_\Delta = 5\ Hz$ refer to (5.6). The following examples illustrate the function of the proposed method's data selection and spectrum analysis blocks.

The example of data selection is shown in Figure 7.4. The sinusoidal motion profile, which includes various motor speeds, was applied during the experiment.

Figure 7.4 shows time marks at the end of selected data segments. The amplitude of the indicating signal is multiplied by two for better visibility. Notice that indicating signal is high after rapid changes in current and low when the signal is uniform; selected areas were used for spectrum analysis.

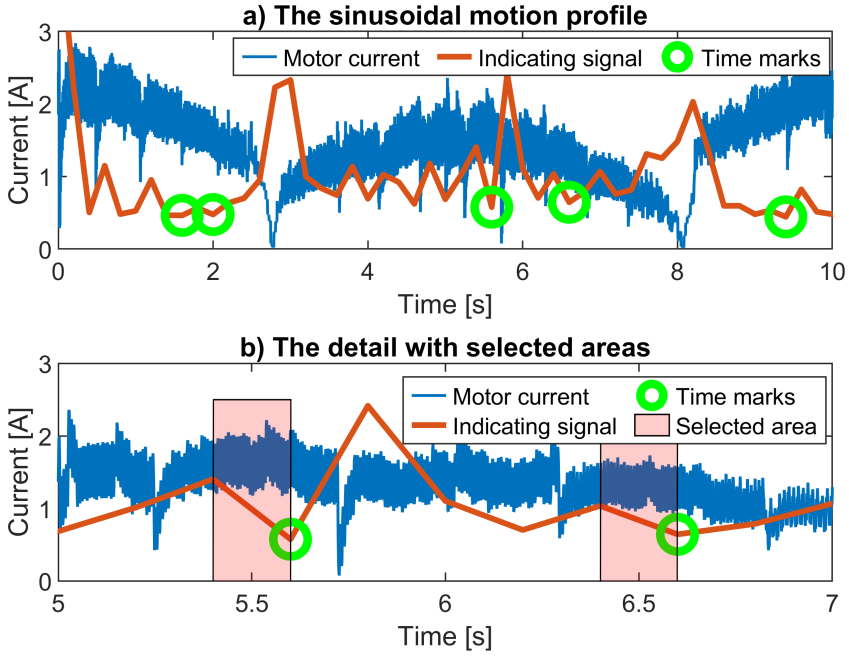

Figure 7.4: The example of data selection based on indicating signal

The example of analysis with three different cases is depicted in Figure 7.5. The "Low speed" case shows a situation where the frequency found in the required range is, in fact, the second harmonic commutation frequency. Therefore, the algorithm continuously checks whether the significant peak is at half the value of the found peak to detect the fundamental commutation frequency correctly. Winding short detection is based on searching for the significant amplitude at twice f_M. Figure 7.5 shows the case of winding short where the significant amplitude should be at frequency $f_{ws} = 2 \cdot f_C/N_C = 2 \cdot 430/8$, thus $f_{ws} = 107.5\ Hz$. The peak at $105\ Hz$ reveals the winding short. The threshold defining fault was set at amplitude as $X_{ws} = X(f_c/2)$. The height of f_{ws} is three times more than f_c, indicating the distinctive extent of the damage. The amplitude of f_{ws} is an important diagnostic parameter. Even if the defined threshold is not exceeded, the fault amplitude can be used to monitor gradual degradations. The "No defect" case shows no significant peak lower than commutation frequency, which means no fault is present. The algorithm also excludes inappropriate data from analysis when the speed of the motor varies. Varying speed is exhibited by the low amplitude and smeared peak of examined frequency. The measurements showed that a sharp peak during nominal operation is usually more than

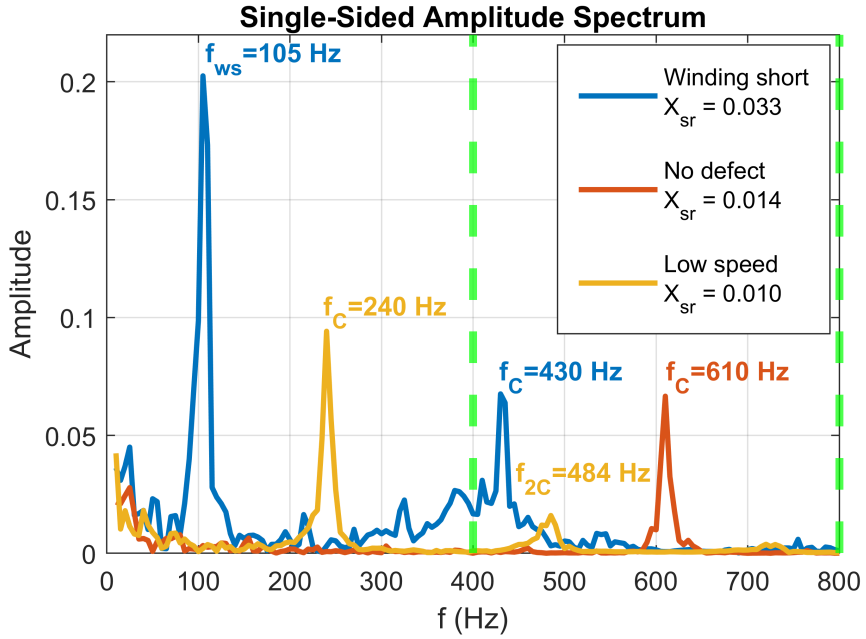

Figure 7.5: The amplitude spectrum analysis where f_C are fundamental commutation frequencies, f_{2C} is second harmonic of f_C and f_{ws} is winding short fault. The area between dashed lines represents the required speed range (50-100% in this case) for which calculated X_{sr} thresholds are displayed. X_{ws} threshold is defined as half of the f_C amplitude

ten times higher than the mean value; therefore, the threshold X_{sr} was set to quintuple of the mean value. Thresholds are always calculated for each case individually, which can be seen in Figure 7.5.

Three outcomes from method testing are shown in Figure 7.6. This example shows one period of rectangular, sinusoidal and triangular motion profiles. Green, red or grey highlighted stripes are areas selected by the data selection algorithm. Green areas are evaluated as nominal, red areas are assessed as faulty, and grey regions contain data that has been excluded from fault detection due to the low or unstable speed of the motor. Figure 7.6 a) shows the output of the detection method during nominal operation. The rectangular motion profile, which includes areas where the actuator holds the target position, was applied during the experiment. These areas are not suitable for fault detection, and therefore they have been automatically excluded from the processing. The relevant areas are evaluated as nominal. Figure 7.6 b) and c) show examples of sinusoidal and triangular movement with winding short faults (a) Fault 2, b) Fault 1). After three positive fault indications, the winding short failures are acknowledged in both cases.

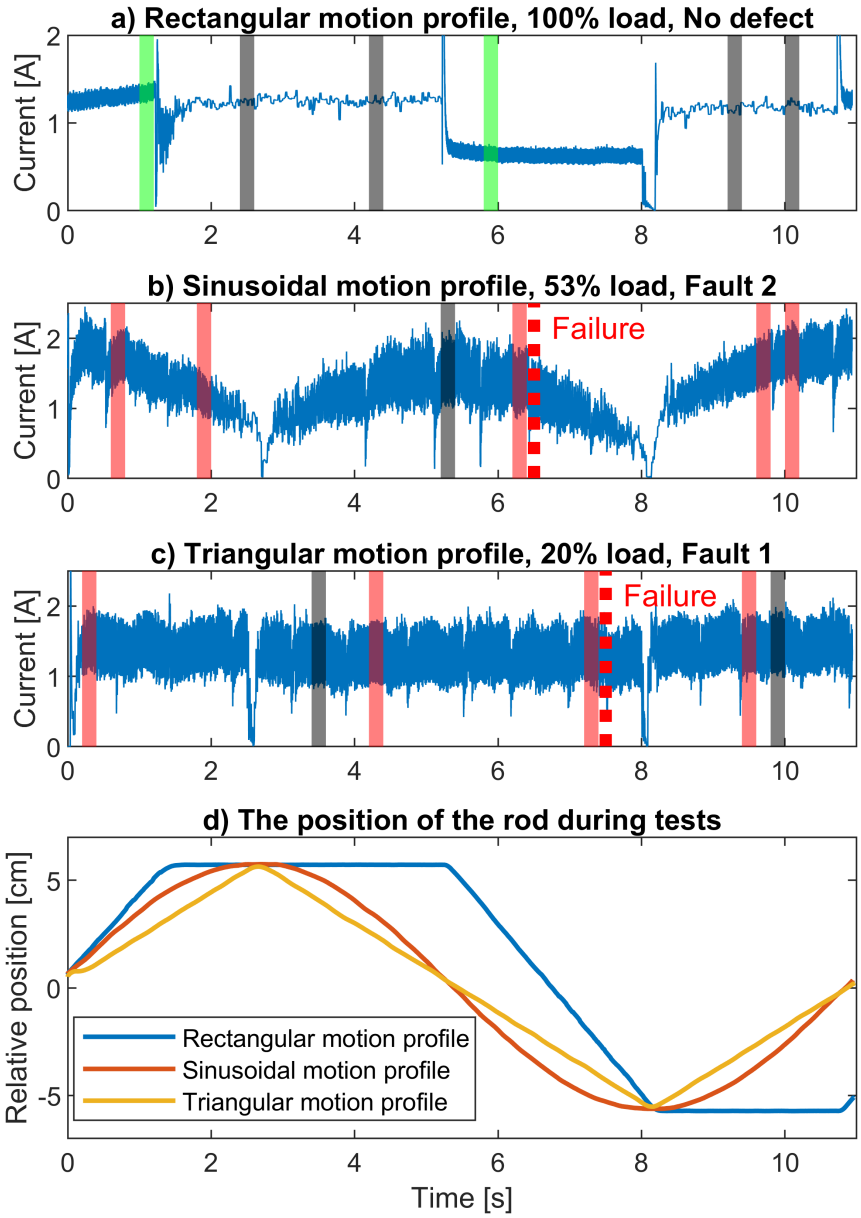

Figure 7.6: Example of outcomes from winding short detection algorithm (a, b, c) and position of actuator's rod recorded during these experiments (d). Highlighted stripes represent the data blocks selected for spectrum analysis, and their colour indicates results: green - no fault detected, red - winding short detected, grey - data excluded from fault detection analysis (low or changing motor speed), red dashed stripe - fault confirmed

7.2 Evaluating of methods

The proposed methods were consistently tested to verify reliability and durability. Each method was tested for the reliability of the fault detection, the sensitivity to input parameters and resistance against noise and disturbing signals.

Since the presented approach is based on detecting commutation spikes in the electric current signal, interference of this signal component can cause significant issues. Because each of the methods processes the data differently, it is possible to expect a different impact of the interference on the detection capabilities.

The introduction of an interfering signal is derived from the amplitude of the commutation spikes, which can take on different values depending on the operating conditions and the actuator's load. In order to cover all operating modes of the actuator, it is necessary to add interference accordingly. The interfering signal is derived from the minimum value of the commutation spikes described in section 5.2. The shape of the commutation spikes can be approximated as a sinusoidal waveform with a fixed RMS value. An interfering signal with various RMS values is added to the current signal. The ratio between RMS of minimum commutation spikes and interference signals is expressed in percentage. The specific values are related to the parameter Xpp (Xpp is 50% of minimum commoutatuion spikes, see section 7.1.1), which corresponds to $2 \cdot X_{ppRMS} = 70.7 mA$. Thus, for example, if 50% of the interference signal is applied, it means that an interference signal of $I_{RMS} = 35.35\, mA$ has been added to the current signal. This procedure is applied both in the case of white noise and the disturbing signal.

7.2.1 Evaluating of jam method

7.2.1.1 Test of fault detection capabilities

The proposed method was tested and evaluated using 35 records of nominal (no fault injected) operation and 34 records containing jam fault. Each test was performed under different operating conditions. The duration of the jam fault was higher than 500 ms in 31 records, two had jam shorter than 300 ms, and one had jam fault between 300 and 500 ms. The confusion matrices in Figure 7.7 summarise the ability of the presented method to detect faults.

7.2.1.2 Sensitivity to input parameters

The method uses three measured motor parameters that could vary for individual motors piece by piece. The effect of variability T_{max} and minimal of peak-to-peak and averaged current were tested. The experiments were performed for each of the tested parameters separately. Individual parameters were examined in the range of 5 to 195% of the correct measured value. Testing was conducted for a set of 32 nominal records and 32 records with jam fault. The set of records was selected to be always correctly evaluated at 100% of the tested parameter. All experiments were conducted for $T_o = 0.3s$. The results from the experiments are shown in Figure 7.8.

a)

0.5 s	Detected state: Nominal	Detected state: Fault
True state: Nominal	35	0
True state: Fault	3	31

b)

0.3 s	Detected state: Nominal	Detected state: Fault
True state: Nominal	35	0
True state: Fault	2	32

c)

0.1 s	Detected state: Nominal	Detected state: Fault
True state: Nominal	33	2
True state: Fault	0	34

Figure 7.7: Confusion matrices for jam detection with different evaluation times: a) 0.5 seconds, b) 0.3 seconds, c) 0.1 seconds

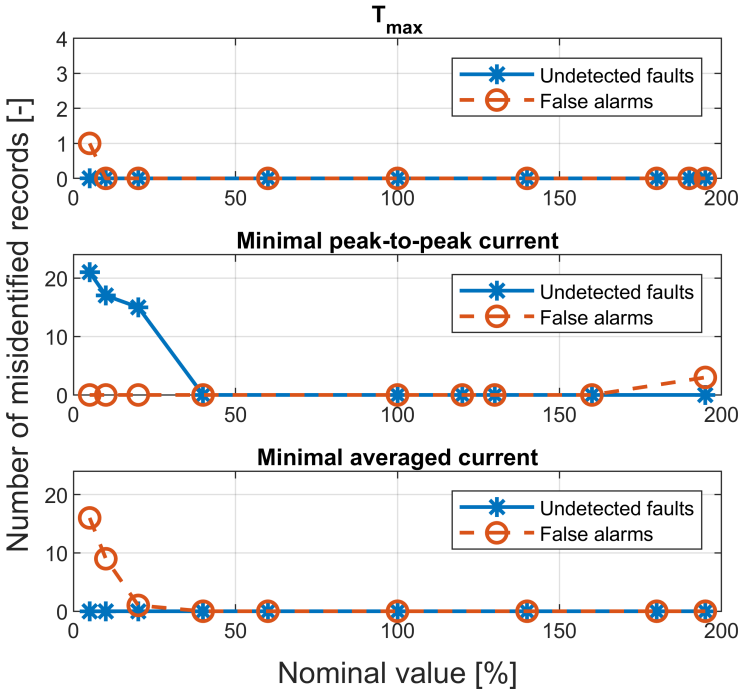

Figure 7.8: Influence of input parameters of the jam detection method

7.2.1.3 Influence of noise

The jam detection method uses the oscillation of the commutation spikes to evaluate the movement of the motor. If the measured current is loaded with noise, a jam fault may stay undetected. The presented detection method uses averaging elements, which can partially suppress the effect of noise, but it can be assumed that at high values, averaging will no longer be sufficient. Therefore, white Gaussian noise was added to the measured signal, and its efficient value was gradually increased to the point where detection failed. The experiment was performed on a data set as described in section 7.2.1.2. The experiments showed that the detection starts to fail if the RMS noise values are higher than 56%. An example of a signal with noise is shown in Figure 7.9.

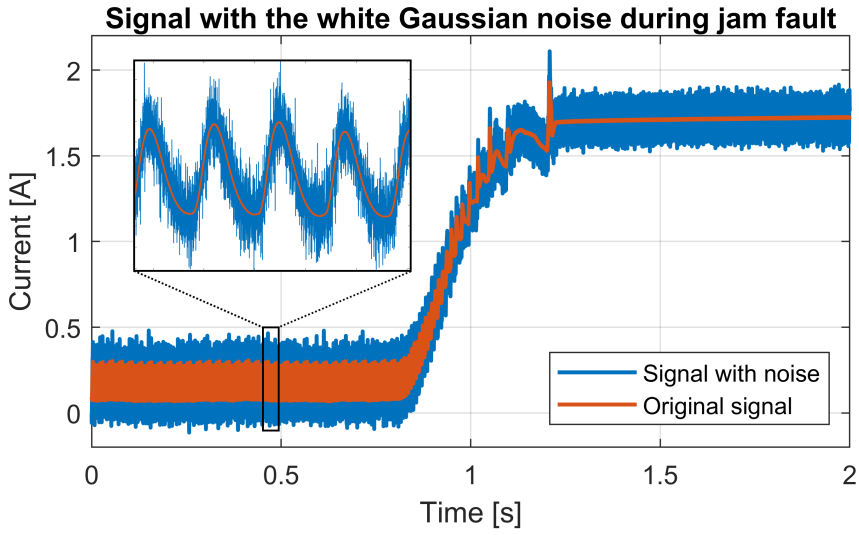

Figure 7.9: Comparison of the nominal and noisy signal during jam fault

The depicted example shows a case where the noise was at 56%, which is the maximum allowable noise value at which the algorithm could work reliably. The high noise amplitudes in the picture indicate an extreme case that should not occur in a real environment. Adding noise to the signal can cause that jam faults may be undetected, but it does not cause false alarms during nominal operation.

7.2.1.4 Influence of disturbing signal

The presence of a disturbing signal can fundamentally affect detecting faults. As with white noise, a disturbing signal can affect the commutation spike signal, making it impossible to detect a jam fault. Unlike white noise, the disturbing signal can suppress the commutation spike if it has the same amplitude and frequency but the opposite phase. In this rare case, false alarms could occur during the nominal operation of the actuator.

The block diagram in Figure 5.2 and equation (5.1) described in section 5.2 indicate that the jam failure detection algorithm can withstand disturbance signals with a frequency

equal to and higher than f_P thanks to averaging. The main concerns are frequencies lower than f_P, and therefore their effect was examined. Disturbing sine signals with a specific frequency and gradually increasing amplitude were added to the measured signal to find the threshold where fault detection fails. The results are summarised in Table 7.3.

Table 7.3: Maximum allowable levels of disturbing signals for the jam detection method

Frequency	50 Hz	400 Hz	1 kHz	4 kHz	8 kHz	16 kHz
RMS of dist. signal	19%	16%	17%	56%	80%	>1000%

The Table shows that frequencies of a periodic signals close to f_P and higher (in this case, 16 kHz) do not affect the fault detection capability. The problem occurs when the frequency of the disturbing signal approaches the frequency range of the commutation spikes. In this area, even low amplitudes of the disturbing sing can significantly reduce detection reliability. This effect can be partially suppressed by changing some parameters of the algorithm. Equations (5.1) and (5.3) show that it is possible to increase parameter a, which is the factor that extends averaging, provided that condition 7.1 is not violated:

$$\frac{1}{f_c} > \frac{a}{f_P} \tag{7.1}$$

where f_P is the maximum commutation frequency for specific actuator. Also, threshold X_{pp} that is by default set to 50% of minimal commutation spikes (see section 5.2) can be increased. However, disturbing signals at frequencies in the range of commutation spikes cannot be entirely suppressed by the algorithm, and their possible occurrence must be mitigated by proper shielding and grounding. The example of such a signal is depicted in Figure 7.10. In this case, a 50 Hz signal was added, a typical example of power lines

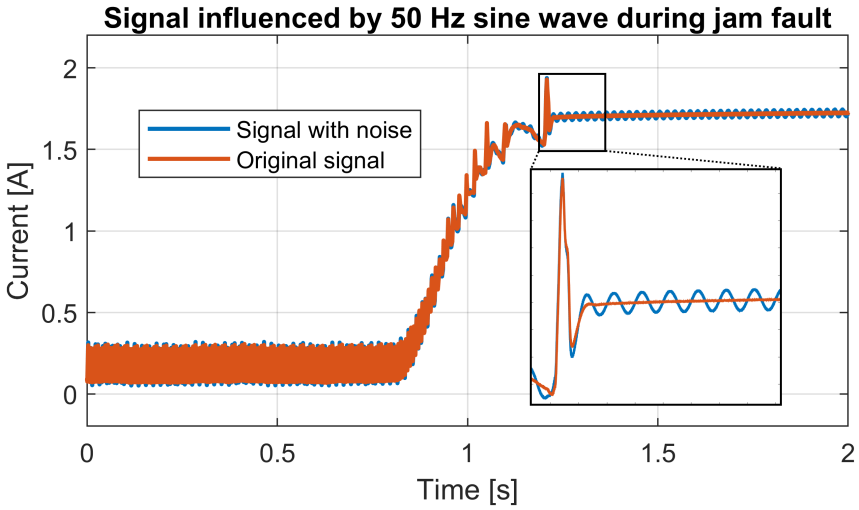

Figure 7.10: Disturbing signal at 50 Hz during jam fault

interference. The RMS of disturbing signal is only 19% of minimal commutation spikes, which is also the highest acceptable level at which the detection procedure still works.

7.2.2 Evaluating of winding short method

7.2.2.1 Test of fault detection capabilities

The fault detection ability of the proposed method was evaluated by a set of experiments. The set consisted of 24 nominal records, 12 with Fault 1 and 12 with Fault 2. Figure 7.11 summarises the ability to detect faults after a certain time.

a)

8 s	Detected state: Nominal	Detected state: Fault
True state: Nominal	24	0
True state: Fault	8	16

b)

11 s	Detected state: Nominal	Detected state: Fault
True state: Nominal	24	0
True state: Fault	3	21

c)

14 s	Detected state: Nominal	Detected state: Fault
True state: Nominal	24	0
True state: Fault	0	24

Figure 7.11: Confusion matrices for winding short detection with different record lengths used for evaluation of fault detection: a) 8 seconds, b) 11 seconds, c) 14 seconds

7.2.2.2 Sensitivity to input parameters

An essential input parameter of the method is the maximum RPM. This parameter may vary slightly for individual motors, and therefore the influence of RPM has been further investigated. The effect was tested on a set of 24 nominal records and 24 records containing winding short faults. Each of the records was 44 seconds long. The parameter was placed between 70 and 130% of the correct value during testing. The result of the experiment is shown in Figure 7.12.

7.2.2.3 Influence of noise

The test of sensitivity to white Gaussian noise was performed in the same way as in the case of a jam failure (see section 7.2.1.3), on the same data set as in section 7.2.2.2. The main difference between the two methods is that while jam failure detection is performed only in the time domain, winding short detection utilises both the time and frequency

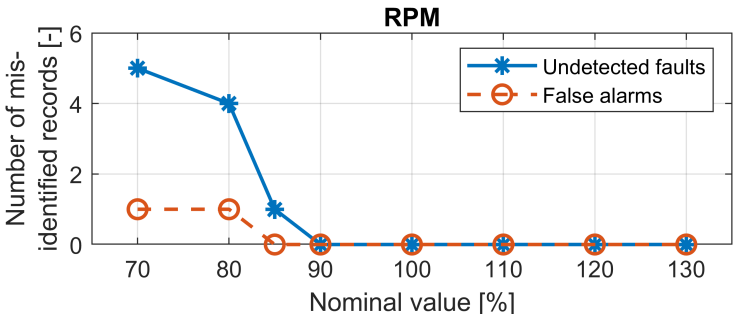

Figure 7.12: Influence of input parameter of the winding short detection method

domains. The white Gaussian noise affects each domain differently, as shown in Figures 7.13 and 7.14.

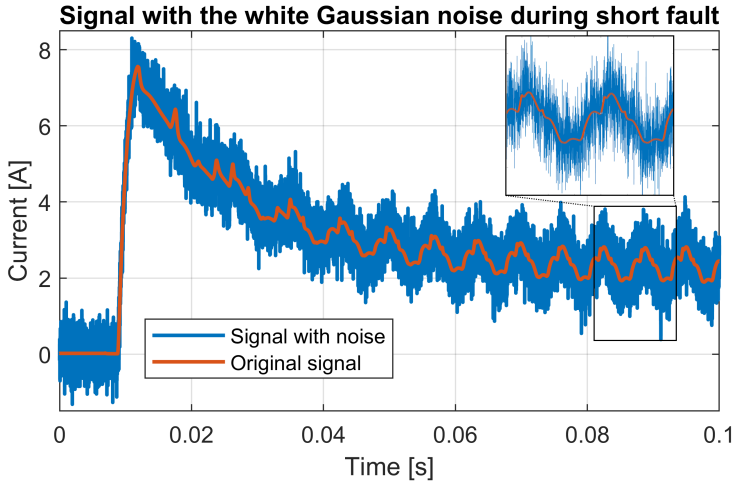

Figure 7.13: Comparison of the nominal and noisy signal during short fault

The experiments showed that the detection starts to fail if the RMS noise values are higher than 540%. The figures demonstrate the different effects of noise. While the time domain is heavily loaded with noise, no fundamental difference is seen in the frequency domain. These findings suggest that the main reason for failure detection is selecting data for diagnosis, which is performed in the time domain. Improperly selected data cannot be effectively evaluated in the subsequent frequency analysis, failing the whole process. It can be assessed that white noise does not pose a significant risk for the jam detection method, as it only failed at very high noise levels, as shown in Figure 7.13.

7.2.2.4 Influence of disturbing signal

The presence of a disturbing signal can fundamentally affect the ability to detect a winding short fault correctly. In addition to affecting the selection of data for analysis, such a

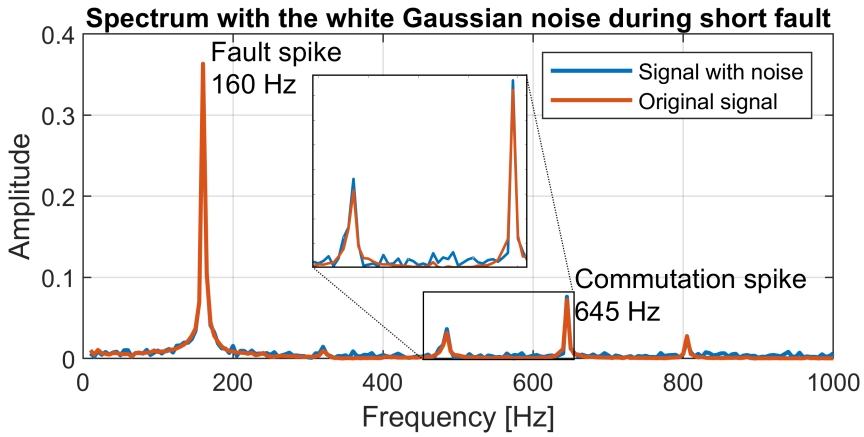

Figure 7.14: Comparison of the nominal and noisy spectrum during short fault

signal can also disrupt the spectral analysis by which the fault is detected. The influence was tested in a similar way as in section 7.2.1.4 using the data set described in section 7.2.2.2. Experiments showed that interfering frequencies located in an analysed part of the spectrum represent a significant concern. Table 7.4 shows the frequencies and levels of the various signals at which the fault detection failed either by the false alarm or undetected failure.

Table 7.4: Maximum allowable levels of disturbing signals for the winding short detection method

Frequency	50 Hz	400 Hz	800 Hz	1 kHz	4 kHz
RMS of dist. signal	>1000%	160%	13%	480%	>1000%

The frequency spectrum analysis takes place in the range given by the actuator parameters. In the specific case, it ranges from 200 Hz to 1 kHz. As can be seen from Table 7.4, the interfering frequencies tested outside this range did not affect the detection capabilities of the method. During 50 Hz and 4 kHz interference, the method worked nominally even at very high noise levels. Other disturbing signals in the defined range significantly reduced the detection capabilities. Their occurrence in the signal causes the algorithm to be unable to recognise individual frequencies in the spectrum correctly. An example of such a confusion is shown in Figure 7.15. The record was measured during a sinusoidal actuator movement, and the value of the inserted disturbing signal was set to 14%. The disturbing signal at 800 Hz was incorrectly identified as the commutation frequency of the motor, which led to incorrect detection of winding short fault. The effects of interfering signals can be partially suppressed by setting higher detection thresholds (X_{se} and X_{ws}), but they cannot be eliminated. When applying the detection system in real operation, it is necessary to ensure adequate shielding. The detection method is susceptible to disturbing signals in the investigated region of the spectrum, the effects of which may reduce the reliability.

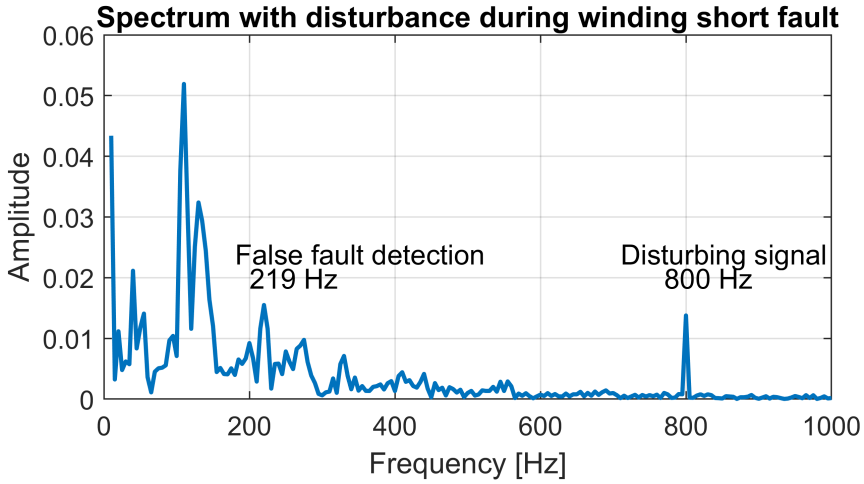

Figure 7.15: Disturbing signal at 800 Hz during short winding fault

7.3 Comparison with existing methods

The non-intrusive approach applied in this thesis brings some benefits over conventional techniques. The presented methods can be individually compared with existing methods in order to evaluate their properties.

Various data-based methods are dealing with the jamming of EMA. Their overview can be seen in [39]. The main disadvantage is that they require the attachment of additional sensors to measure parameters such as temperature, vibration or position [2], [26]. In contrast, the proposed non-intrusive approach that utilises only the actuator's current and basic electromechanical properties is easy to implement because the current measurement is available directly on the motor driver.

In the case of winding shorts, there are some methods for faults detection in EMA with BLDC motors [11], [30]. Due to the different electrical excitation of the winding, the manifestation of faults is entirely dissimilar, and these methods cannot be used for EMA with brushed DC motors. For a brushed DC motor, there are some hidden Markov Model (HMM)-based methods [38]. Unlike the proposed methods, these techniques use a supervised learning approach, which is a significant disadvantage preventing use in industry.

The proposed methods are also able to deal with the dynamic behaviour of EMA operation. The jam detection method uses dynamic changes during operation to evaluate the movement of EMA, while the winding short fault detection method utilises a novel approach to distinguish in which sections of the signal the analysis should be performed. In contrast to other techniques that utilise additional sensors or procedures, such as various order tracking or machine learning methods, the proposed approach does not require supplementary information sources and complex implementations. Therefore it can be implemented in embedded devices such as generic 200 MHz microcontrollers for near to real-time fault detection.

7.4 Summary of results

The developed methods have been tested under various conditions, including different profiles of motion, speeds or loads. The tests included a simulation of the defects to which the methods were exposed. The jamming methods were tested using a mechanical stop with which it was possible to test sharp and gradual jamming. The winding short detection method was verified by artificially introducing two different short-circuit faults into the actuator motor rotor. The experiments aimed to check the behaviour of the proposed methods in individual steps and evaluate their properties, which are summarised in the following sections.

7.4.1 Fault detection ability

Both methods are equipped with fault evaluation procedures that help to avoid the incorrect classification. The jam detection method uses the evaluation time T_o. With a rising T_o (see Figure 7.7 a), the method identifies nominal states correctly. However, events with fault-like states shorter than T_o were not detected. An example of a fault-like state can be the effect of static friction during the run-up at high loads. The actuator shows signs of jamming until the static friction is overcome and this phenomenon disappears. The low value of T_o helps to discover even these states, but it might cause false alarms (see Figure 7.7 c). The value of T_o should be set individually according to the required detection sensitivity. The fault evaluation procedure of the winding short detection method ensures that the method classifies nominal records correctly, but it delays the fault confirmation. The incorrectly classified states may occur when the spectrum analysis cannot correctly identify commutation frequency due to low or unstable motor speed. The method correctly identified faults in 16 out of 24 records after 8 seconds, 21 records after 11 seconds and the rest within 14 seconds. The results confirm that the ability to detect fault increases with time.

7.4.2 The speed of detection

The speed of fault detection is different for each of the proposed methods. In the case of jam detection, the time to detect fault is given by the evaluation time. The evaluation time can be set individually to meet the requirements of the specific application however it was never longer than half of a second during experiments (see Figure 7.7). In the case of winding short detection, the time of fault detection depends on the extent of the failure, chosen thresholds, and the most on the actuator's operation conditions. The fault detection is analysed once in the defined period, and the fault evaluation needs multiple conformations. Therefore the time to detect fault can vary in the range of units to tens of seconds (see Figure 7.11). Even though the fault may not be confirmed immediately, it is possible to monitor its development. The amplitude in spectrum analysis that corresponds to the winding short can be examined to assess the severity of the defects.

The jam detection method is able to detect faults in the entire range of speeds for the given actuator. The winding short detection works reliably for at least 25% of the maximum motor's speed and higher. At rates below 25%, the resolution of the individual frequencies is not reliable; therefore, these data are excluded from the analysis.

7.4.3 Sensitivity to input parameters

The proposed methods use various electromechanical properties of actuators, which may not be constant in real conditions. The influence of the variability of the input parameters was verified experimentally. In the case of the jam detection method, three input parameters were examined. Experiments have shown that the method works correctly from 40 to 160% of all three parameters. In the case of the winding short detection method, the maximum speed of the motor has been identified as an essential input parameter. The method worked adequately in the range of 90 to 130%. The values under 90% represent cases where the unloaded motor has higher RPM than expected, and the method may raise false alarms or misidentified faults. However, the loaded actuator tends to operate slower, and therefore this limitation is not crucial.

7.4.4 Sensitivity to noise

Interference immunity was tested using two experiments. The methods were exposed to white Gaussian noise and disturbing signals with different frequencies. The sensitivity of each method to different noise levels varied, which is due to distinct signal processing. It can be concluded that methods resist white noise well, and the detection failure occurs only at very high levels. However, they are sensitive to disturbing signals with specific frequencies. When disturbing signal interfere commutation spikes that both methods utilise for fault detection, the reliability decreases. Although this effect can be partially eliminated by changing threshold parameters, it is impossible to eliminate it. Therefore, in real operation, it would be necessary to use other means, such as adequate shielding and grounding, to suppress the effect of disturbing signals.

Chapter 8

Conclusions

8.1 Summary

This thesis deals with the issue of monitoring, fault of detection and degradation of electromechanical actuators. The main goal was to create diagnostic methods for an EMA with a brush DC motor, using a non-intrusive approach. This goal was achieved by diagnostic based on measurement of motor current. Compared to conventional methods, the main advantage of this approach is that it does not require additional sensors attached to the actuator, thus any unnecessary interventions. The thesis proposes methods for detecting actuator jam and motor winding short that utilise unique properties of the current signal of the brush DC motor. Presented methods are designed to deal with the dynamic behaviour of EMA during various operating modes doing so without any other additional sensors or sources of information. Thanks to the non-intrusive approach and low computational complexity, methods are easy to implement in industrial applications utilising the EMAs.

8.2 Accomplishment of Thesis specific aims

- **Analysis of specific EMA faults (more details in chapter 4):** The first objective was to process a detailed analysis of faults that may occur with an electromechanical actuator with a brush motor. The analysis focused on the actuator's basic building blocks and its components. Its main goal was to identify individual defects and degradations and to investigate the mechanisms leading to failure. The most common mechanisms, including heat effects, mechanical overload, vibration, pollution, insufficient lubrication, manufacturing defects and environmental influences, were investigated. The effects of these mechanisms vary depending on the specific component. Therefore, the analysis was supplemented with information about monitoring possibilities of the occurrence and extent of these defects. Besides the basic actuator blocks, additional components such as sensors and control electronics were

also processed. The analysis includes a Table summarising the relative probability and criticality of faults.

- **Design of fault detection methods (more details in chapter 5):** The main objective was the design of fault detection methods. The thesis deals with the actuator jam and winding short motor fault. Investigated faults were selected based on the proposed analysis, the specific properties of the current signal in the brush DC motor, and the non-intrusive approach's requirements. Both proposed methods use mechanisms to reduce computational complexity and increase the reliability of fault detection. The jam detection method monitors the presence of commutation spikes in the current signal and compares it with the average current value. Based on these parameters, it can evaluate whether the actuator has jammed independently of the operating conditions. The winding short detection method monitors the electrical balance using commutation spikes. A winding short fault results in an increase in spikes twice per engine revolution. Evaluation of this phenomenon is possible only in the steady operation of the actuator. For this purpose, the method uses a specially designed procedure that preprocesses the data and evaluates which blocks will be suitable for analysis.

- **Design of testing system for EMA (more details in chapter 6):** The proposed methods had to be tested and verified. For this purpose, an automated test system was designed and constructed. The system consists of an aluminium frame, a linear guide and mounting parts of individual components such as actuators and sensors. The tested actuator can be loaded by static weights or an actively controlled secondary actuator. An automated course of the tests is controlled using software in the LabView environment that drives control units in the form of H-bridges by PWM pulses. During the experiments, parameters such as absolute position, force, voltages, currents, temperatures, vibrations and motor speed are measured. Data provided by the system are processed and can be utilised to test and evaluate diagnostics methods.

- **Testing of proposed methods (more details in chapter 7.1):** Both methods have been thoroughly tested to verify their ability to detect defects under different operating conditions. The jam failure was simulated by a mechanical obstacle in which the actuator struck at different speeds and forces. The winding short circuit fault was simulated by artificially introducing two types of shorts into the actuator rotor winding. The damaged actuator was then operated with different loads in variable operating modes. The data measured during these experiments were used to validate and improve the performance of the proposed methods. Experiments show that both proposed methods can reliably detect faults in different operating conditions. The speed of fault detection was in the order of hundreds of milliseconds in the case of the jam fault and units of seconds in the case of the winding short.

- **Evaluation of method properties (more details in chapter 7.2):** The properties of the proposed methods were investigated during tests that simulated situations in which they may fail. These tests included experiments verifying sensitivity to the variability of input parameters and resistance to noise and disturbing signals. The jam detection method proved to be sufficiently resistant to the variability of input parameters and noise. The winding short detection method is also resistant to noise, but it may fail in the unlikely event when the motor RPM is higher than anticipated. The main concern for both methods represents the disturbing signals that may interfere with commutation spikes. Their effect must be suppressed by adequate shielding and grounding.

8.3 Future Work

Future work can go in two directions. The first direction may be the further development of non-intrusive approaches. Measurement and processing of electrical voltage in combination with current can significantly expand the number of detectable faults. The disadvantage is that thanks to the control of the actuator using PWM, sampling at higher speeds than in the current form would be required for voltage processing, which would create higher system requirements.

The second direction could be employing sensors, which some actuators may be equipped with. In addition to the commonly used position sensor, it would be possible to focus on the IRC sensor. Since IRC provides information about the position of the motor's shaft, it is possible to use it to monitor other related parameters, such as angular velocities and accelerations, which can be converted to the information related to the gearbox and leading screw. In addition, IRC appears to be an ideal element helping to eliminate the problems associated with time-domain measurements. Sampling or processing of data in the position domain brings several advantages in various order analyses, which help suppress the problems associated with the variability of the motor speed.

In addition to the real-time fault evaluation primarily investigated in this thesis, it is also possible to process and compare historical data. This approach makes it possible to monitor system degradations' occurrence and gradual development and is an ideal source of information for predictive systems monitoring equipment life.

Bibliography

[1] G. C. Stone, *Electrical insulation for rotating machines, design, evaluation, aging, testing, and repair*. Hoboken, NJ: Wiley-Interscience, c2004, ISBN: 04-714-4506-1.

[2] D. S. Bodden, N. S. Clements, B. Schley and G. Jenney, "Seeded failure testing and analysis of an electro-mechanical actuator," *2007 IEEE Aerospace Conference*, 2007. DOI: 10.1109/aero.2007.352880.

[3] S. Ruoho, E. Dlala and A. Arkkio, "Comparison of Demagnetization Models for Finite-Element Analysis of Permanent-Magnet Synchronous Machines," *IEEE Transactions on Magnetics*, vol. 43, no. 11, pp. 3964–3968, Nov. 2007, ISSN: 1941-0069. DOI: 10.1109/TMAG.2007.906749.

[4] M. Sinnett, "787 no-bleed systems: Saving fuel and enhancing operational efficiencies," *AERO Magazine*, vol. 7, no. 4, pp. 6–11, 2007.

[5] D. Allen, W. Przytula, J. Vian and G. Mansouri, "Health monitoring for commercial aircraft systems," *ICAS Secretariat - 26th Congress of International Council of the Aeronautical Sciences 2008, ICAS 2008*, vol. 4, Jan. 2008.

[6] E. Balaban, P. Bansal and P. Stoelting, "A diagnostic approach for electro-mechanical actuators in aerospace systems," *2009 IEEE Aerospace conference*, vol. 2009, 2009. DOI: 10.1109/AERO.2009.4839661.

[7] M. Smith, C. Byington, M. Watson *et al.*, "Experimental and analytical development of health management for electro-mechanical actuators," in *2009 IEEE Aerospace conference*, Apr. 2009, pp. 1–14. DOI: 10.1109/AERO.2009.4839660.

[8] A. Behbahani and K. Semega, "Control strategy for electro-mechanical actuators versus hydraulic actuation systems for aerospace applications," *SAE Technical Papers*, Nov. 2010. DOI: 10.4271/2010-01-1747.

[9] J. Gieras, *Permanent Magnet Motor Technology: Design and Applications*, 3rd. CRC Press, Jan. 2010, pp. 4–6, ISBN: 978-1-4200-6440-7.

[10] P. Nemecek and E. Tomeh, *Vibracní diagnostika základních závad stroju*, 1st ed. Technická univerzita v Liberci, 2010.

[11] K. Yu, F. Yang, H. Guo and X. Jinquan, "Fault diagnosis and location of brushless dc motor system based on wavelet transform and artificial neural network," *2010 International Conference on Electrical Machines and Systems, ICEMS2010*, Jan. 2010.

[12] J. Brombach, T. Schroter, A. Lucken and D. Schulz, "Optimized cabin power supply with a +- 270 v dc grid on a modern aircraft," *2011 7th International Conference-Workshop Compatibility and Power Electronics (CPE)*, pp. 425–428, 2011. DOI: 10.1109/CPE.2011.5942274.

[13] X. Roboam, "New trends and challenges of electrical networks embedded in "more electrical aircraft," *2011 IEEE International Symposium on Industrial Electronics*, pp. 26–31, 2011. DOI: 10.1109/ISIE.2011.5984130.

[14] A.-H. Ahmed, "Power generation and distribution system for a more electric aircraft - a review," *Recent Advances in Aircraft Technology*, pp. 289–308, Feb. 2012. DOI: 10.5772/37290.

[15] D. Li and X. Li, "Study of degradation in switching mode power supply based on the theory of pof," *2012 International Conference on Computer Science and Service System*, 2012. DOI: 10.1109/csss.2012.493.

[16] M. Ristanović, Žarko Ćojbašić and D. Lazić, "Intelligent control of dc motor driven electromechanical fin actuator," *Control Engineering Practice*, vol. 20, no. 6, pp. 610–617, 2012, ISSN: 0967-0661. DOI: https://doi.org/10.1016/j.conengprac.2012.02.009.

[17] I. Chirico Anthony J. and J. R. Kolodziej, "A Data-Driven Methodology for Fault Detection in Electromechanical Actuators," *Journal of Dynamic Systems, Measurement, and Control*, vol. 136, no. 4, Apr. 2014, ISSN: 0022-0434. DOI: 10.1115/1.4026835.

[18] P. Diouf and W. Herbert, "Understanding rotor balance for electric motors," *Conference Record of 2014 Annual Pulp and Paper Industry Technical Conference*, 2014. DOI: 10.1109/ppic.2014.6871143.

[19] J. Neuzil, O. Kreibich and R. Smid, "A distributed fault detection system based on iwsn for machine condition monitoring," *IEEE Transactions on Industrial Informatics*, vol. 10, no. 2, pp. 1118–1123, 2014. DOI: 10.1109/TII.2013.2290432.

[20] P. H. Westfall, "Kurtosis as peakedness, 1905 - 2014.r.i.p.," *The American Statistician*, vol. 68, no. 3, pp. 191–195, 2014. DOI: 10.1080/00031305.2014.917055.

[21] D. Barater, G. Buticchi, A. Soldati *et al.*, "Multistress characterization of insulation aging mechanisms in aerospace electric actuators," *2015 IEEE Energy Conversion Congress and Exposition (ECCE)*, pp. 2215–2222, 2015. DOI: 10.1109/ECCE.2015.7309972.

[22] B. Sarlioglu and C. T. Morris, "More electric aircraft: Review, challenges, and opportunities for commercial transport aircraft," *IEEE Transactions on Transportation Electrification*, vol. 1, no. 1, pp. 54–64, 2015.

[23] M. Todeschi and L. Baxerres, "Health monitoring for the flight control emas," *IFAC-PapersOnLine*, vol. 48, no. 21, pp. 186–193, 2015, 9th IFAC Symposium on Fault Detection, Supervision andSafety for Technical Processes SAFEPROCESS 2015, ISSN: 2405-8963. DOI: https://doi.org/10.1016/j.ifacol.2015.09.526.

[24] D. Xu and S. Sui, "Bivariate degradation modeling and reliability evaluation of accelerometer based on physics- statistics model and copula function," *2015 First International Conference on Reliability Systems Engineering (ICRSE)*, 2015. DOI: 10.1109/icrse.2015.7366408.

[25] C. Yuyan, W. Jian, X. Rong and W. Xinmin, "Fault tree analysis of electro-mechanical actuators," *2015 34th Chinese Control Conference (CCC)*, pp. 6392–6396, 2015. DOI: 10.1109/ChiCC.2015.7260646.

[26] M. A. A. Ismail, E. Balaban and H. Spangenberg, "Fault detection and classification for flight control electromechanical actuators," *2016 IEEE Aerospace Conference*, pp. 1–10, 2016. DOI: 10.1109/AERO.2016.7500784.

[27] J. Li, Z. Yu, Y. Huang and Z. Li, "A review of electromechanical actuation system for more electric aircraft," in *2016 IEEE International Conference on Aircraft Utility Systems (AUS)*, 2016, pp. 490–497. DOI: 10.1109/AUS.2016.7748100.

[28] J. Yang, Z. Yang and X. Sun, "Modeling and fault analysis of brushless dc motor for electromechanical actuator," *2016 IEEE International Conference on Aircraft Utility Systems (AUS)*, Oct. 2016. DOI: 10.1109/aus.2016.7748173.

[29] D. Arriola and F. Thielecke, "Model-based design and experimental verification of a monitoring concept for an active-active electromechanical aileron actuation system," *Mechanical Systems and Signal Processing*, vol. 94, pp. 322–345, 2017. DOI: 10.1016/j.ymssp.2017.02.039.

[30] A. De Martin, G. Jacazio and G. Vachtsevanos, "Windings fault detection and prognosis in electro-mechanical flight control actuators operating in active-active configuration," *International Journal of Prognostics and Health Management*, vol. 8, Jun. 2017. DOI: 10.36001/ijphm.2017.v8i2.2633.

[31] G. Di Rito, F. Schettini and R. Galatolo, "Model-based health-monitoring of an electro-mechanical actuator for unmanned aerial system flight controls," *2017 IEEE International Workshop on Metrology for AeroSpace (MetroAeroSpace)*, pp. 502–511, 2017. DOI: 10.1109/MetroAeroSpace.2017.7999626.

[32] J.-C. MARÉ and J. FU, "Review on signal-by-wire and power-by-wire actuation for more electric aircraft," *Chinese Journal of Aeronautics*, vol. 30, no. 3, pp. 857–870, 2017, ISSN: 1000-9361. DOI: https://doi.org/10.1016/j.cja.2017.03.013.

[33] M. Mazzoleni, G. Maroni, Y. Maccarana, S. Formentin and F. Previdi, "Fault detection in airliner electro-mechanical actuators via hybrid particle filtering," *IFAC-PapersOnLine*, vol. 50, no. 1, pp. 2860–2865, Jul. 2017. DOI: 10.1016/j.ifacol.2017.08.640.

[34] G. Pietrini, D. Barater, F. Immovilli, A. Cavallini and G. Franceschini, "Multi-stress lifetime model of the winding insulation of electrical machines," *2017 IEEE Workshop on Electrical Machines Design, Control and Diagnosis (WEMDCD)*, Apr. 2017. DOI: 10.1109/wemdcd.2017.7947758.

[35] G. Di Rito, F. Schettini and R. Galatolo, "Model-based prognostic health-management algorithms for the freeplay identification in electromechanical flight control actuators," *2018 5th IEEE International Workshop on Metrology for AeroSpace (MetroAeroSpace)*, pp. 340–345, 2018. DOI: 10.1109/MetroAeroSpace.2018.8453552.

[36] F. Previdi, Y. Maccarana, M. Mazzoleni, M. Scandella, G. Pispola and N. Porzi, "Development and experimental testing of a health monitoring system of electromechanical actuators for small airplanes," *2018 26th Mediterranean Conference on Control and Automation (MED)*, 2018. DOI: 10.1109/med.2018.8442734.

[37] C. Ruiz-Carcel and A. Starr, "Data-based detection and diagnosis of faults in linear actuators," *IEEE Transactions on Instrumentation and Measurement*, vol. 67, no. 9, pp. 2035–2047, 2018. DOI: 10.1109/tim.2018.2814067.

[38] J. Zhang, W. Zhan and M. Ehsani, "On-line diagnosis of inter-turn short circuit fault for dc brushed motor," *ISA Transactions*, vol. 77, pp. 179–187, 2018, ISSN: 0019-0578. DOI: https://doi.org/10.1016/j.isatra.2018.03.029.

[39] Y. Hussain, S. Burrow, L. Henson and P. Keogh, "A review of techniques to mitigate jamming in electromechanical actuators for safety critical applications," *International Journal of Prognostics and Health Management*, vol. 9, Dec. 2020. DOI: 10.36001/ijphm.2018.v9i3.2749.

[40] Y. Park, H. Choi, J. Shin, J. Park, S. B. Lee and H. Jo, "Airgap flux based detection and classification of induction motor rotor and load defects during the starting transient," *IEEE Transactions on Industrial Electronics*, vol. 67, no. 12, pp. 10 075–10 084, 2020. DOI: 10.1109/TIE.2019.2962470.

[41] S. B. Lee, J. Shin, Y. Park, H. Kim and J. Kim, "Reliable flux-based detection of induction motor rotor faults from the fifth rotor rotational frequency sideband," *IEEE Transactions on Industrial Electronics*, vol. 68, no. 9, pp. 7874–7883, 2021. DOI: 10.1109/TIE.2020.3016241.

[42] J.-C. Maré, "Review and analysis of the reasons delaying the entry into service of power-by-wire actuators for high-power safety-critical applications," *Actuators*, vol. 10, no. 9, 2021, ISSN: 2076-0825. DOI: 10.3390/act10090233.

Appendix A

List of Publications

A.1 Publications in Journals with Impact Factor Relevant to the Thesis

[1] O. Hanuš and R. Šmíd, "Non-intrusive current-based fault detection of electro-mechanical actuators with brushed dc motor," *Metrology and Measurement Systems*, 2022.

A.2 International Conference Proceedings Relevant to the Thesis

[1] O. Hanuš, "Nilm-based algorithm for load and degradation monitoring," in *Proceedings of the 20th International Scientific Student Conferenece POSTER 2016*, Czech Technical University in Prague, 2016.

[2] O. Hanuš and R. Šmíd, "Automated testing system for electro-mechanical actuators used in aviation," in *24th IMEKO TC4 International Symposium and 22nd International Workshop on ADC and DAC Modelling and Testing*, IMEKO, 2020. [Online]. Available: `http://www.imeko-tc4-2020.org/`.

A.3 Other Publications in Journals with Impact Factor

[1] V. Horyna, O. Hanuš and R. Šmíd, "Virtual mass flow rate sensor using a fixed-plate recuperator," *IEEE Sensors Journal*, vol. 19, no. 14, Jul. 2019. DOI: `10.1109/JSEN.2019.2894526`.

[2] J. Mikeš, S. Pekárek, O. Babčenko, O. Hanuš, J. Kákona and P. Štenclová, "3d printing materials for generators of active particles based on electrical discharges," *Plasma Processes and Polymers*, vol. 17, no. 1, Jan. 2020. DOI: 10.1002/ppap.201900150. [Online]. Available: https://onlinelibrary.wiley.com/doi/full/10.1002/ppap.201900150?af=R.

[3] J. Mikeš, S. Pekárek and O. Hanuš, "Surface dielectric barrier discharge in a cylindrical configuration - effect of airflow orientation to the microdischarges," *Ozone Science and Engineering*, Dec. 2021. DOI: 10.1080/01919512.2021.2016369.

[4] S. Pekárek, J. Mikeš, M. Červenka and O. Hanuš, "Air supply mode effects on ozone production of surface dielectric barrier discharge in a cylindrical configuration," *PLASMA CHEMISTRY AND PLASMA PROCESSING*, vol. 41, no. 3, Jan. 2021. DOI: 10.1007/s11090-021-10154-x. [Online]. Available: https://link.springer.com/article/10.1007/s11090-021-10154-x.

A.4 Other International Conference Proceedings

[1] V. Horyna and O. Hanuš, "Air handling unit test rig for research and development of fault detection and diagnostics methods," in *POSTER 2014 - 18th International Student Conference on Electrical Engineering*, Czech Technical University, 2014.

[2] O. Hanuš and V. Horyna, "Virtual sensor of mass flow for diagnosis of hvac unit," in *The Twelfth International Conference on Condition Monitoring and Machinery Failure Prevention Technologies*, Coxmoor Publishing Co., 2015.

[3] R. Šmíd, V. Horyna and O. Hanuš, "Ontology based automated design of fdd systems," in *The Twelfth International Conference on Condition Monitoring and Machinery Failure Prevention Technologies*, Coxmoor Publishing Co., 2015.

[4] R. Šmíd and O. Hanuš, "Condition monitoring using iot," in *CM 2016 and MFPT 2016*, British Institute of Non-Destructive Testing (BINDT), 2016.

[5] J. Mikeš, O. Hanuš and J. Kákona, "Methodology for monitoring lightning stroke of an object by means of a smart sensoric," in *Proceedings of the International Conference on Lightning & Static Electricity (ICOLSE 2017)*, The Institute of Electrical Engineers of Japan, 2017.

[6] ——, "Piezoelectric lightning current detection," in *4th International Lightning Protection Symposium*, ser. 1, vol. 1, International Lightning Protection Association, 2018.

[7] O. Hanuš, J. Mikeš and J. Kákona, "Autonomous groundwater monitoring station with wireless communication," in *23rd IMEKO TC4 Symposium Electrical & Electronic Measurement*, ser. 23, IMEKO TC4 Technical Committee on Measurement of Electrical Quantities, 2019.

Appendix B

Additional images

B.1 Conditioning circuit

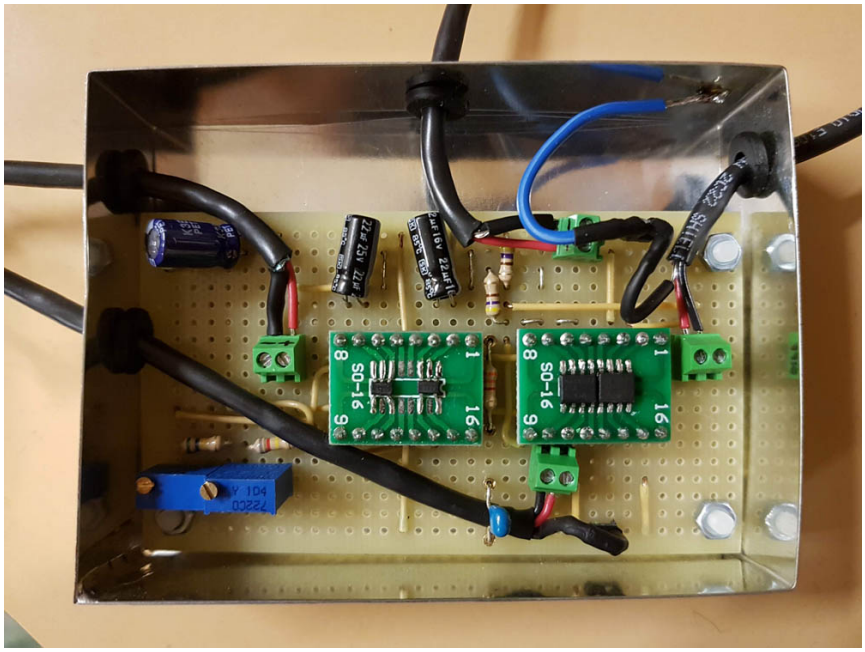

Figure B.1: Conditioning circuit

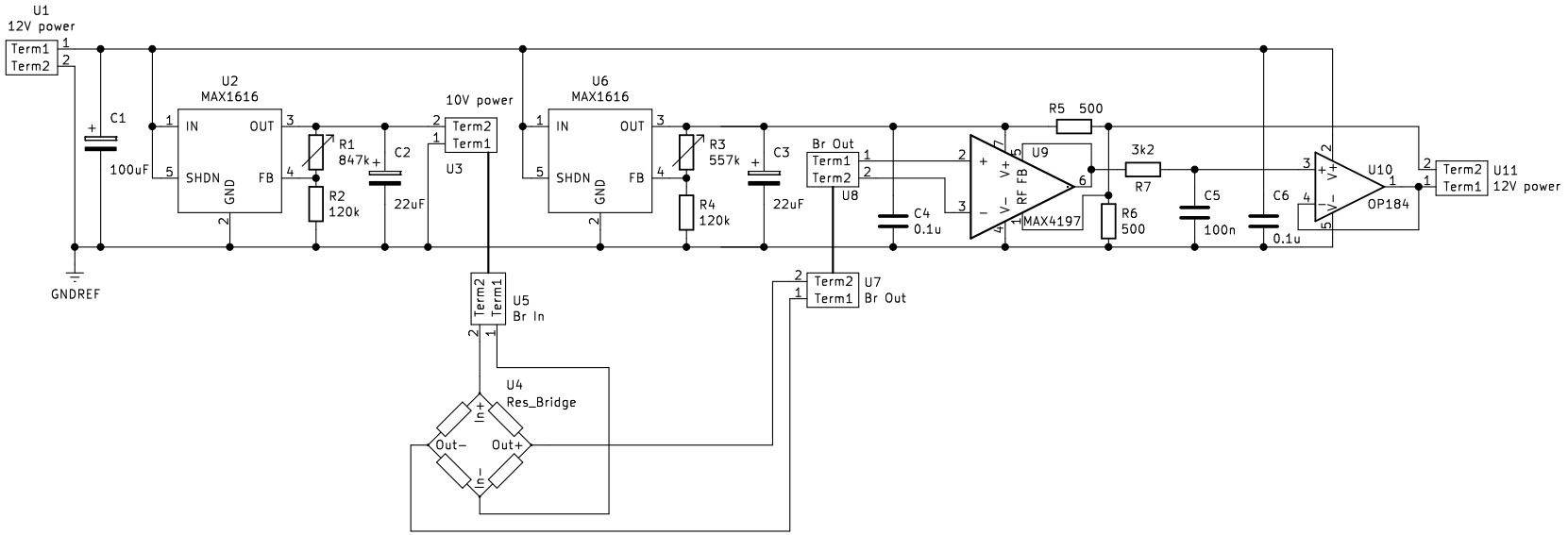

Figure B.2: Schematic of conditioning circuit